Site Preference in Vertex-Sharing Polyicosahedral Supraclusters Containing Group 10 and 11 Metals and Their Bonding Implications: Syntheses and Structures of the First Au–Ag–M (M = Pt, Ni) Biicosahedral Clusters $[(Ph_3P)_{10}Au_{12}Ag_{12}PtCl_7]Cl$ and $[(Ph_3P)_{10}Au_{12}Ag_{12}NiCl_7](SbF_6)$

Boon K. Teo,* Hong Zhang, and Xiaobo Shi

Department of Chemistry, University of Illinois at Chicago, Chicago, Illinois 60680

Received December 27, 1993®

The syntheses and structures of the first Au–Ag–M (M = Pt, Ni) vertex-sharing biicosahedral clusters $[(Ph_3P)_{10}Au_{12}Ag_{12}PtCl_7]^+$ (**1**), as the Cl^- salt, and $[(Ph_3P)_{10}Au_{12}Ag_{12}NiCl_7]^+$ (**4**), as the SbF_6^- salt, are reported. **4** is also the first Au–Ag–Ni compound ever reported as well as the first example of a vertex-sharing polyicosahedral structure containing first, second, and third row transition metals. The title clusters were synthesized via a new synthetic strategy based on preformed clusters; as such, they open the door to other trimetallic polyicosahedral clusters containing group 10 and 11 metals. The title clusters crystallize in a monoclinic unit cell of $P2_1/m$ space group symmetry with lattice parameters a = 16.534(3) Å, b = 24.360(4) Å, c = 29.819(6) Å, β = 103.25(3)°, and V = 11690.3 Å^3 for **1**, as the Cl^- salt, and a = 16.591(4) Å, b = 23.707(3) Å, c = 29.954(5) Å, β = 103.31(3)°, V = 11465.2 Å^3 for **4**, as the SbF_6^- salt, respectively, and Z = 2. The structures were refined to R_1 = 7.0% for 3014 independent reflections ($2\theta \leq 44°$) with $I > 3\sigma$ for **1**, and R_1 = 6.9% for 1822 independent reflections ($2\theta \leq 44°$) with $I > 3\sigma$ for **4**, respectively. The metal core of both structures can be described as two Au_6Ag_6 icosahedra, one M-centered (M = Pt (**1**), Ni (**4**)) and one Au-centered, sharing a common Au atom. The four metal pentagons adopt the staggered–eclipsed–staggered (*ses*) configuration. The ten triphenylphosphine ligands coordinate to the 10 peripheral (surface) Au atoms in a radial fashion. There are five doubly-bridging chloride ligands connecting two Ag_5 pentagons and two more chloride ligands coordinating terminally to two apical Ag atoms. The ubiquity of crystal structures with the space group $P2_1/m$ and cell parameters of, roughly, 16, 24, and 30 Å and β = 103° for the series of vertex-sharing biicosahedral supraclusters with triphenylphosphine as ligands, regardless of the types of counteranions (e.g., SbF_6^- vs Cl^-), halide ligands (e.g., Cl^- vs Br^-), or solvent molecules, is discussed. On the basis of these structures, a set of site preference rules are deduced and their bonding implications discussed. These site preference principles can be generalized to other multimetallic alloy systems and rationalized via simple bond strength vs charge accumulation (BSCA) plots. Here the metal–metal bond strengths are estimated from cohesive energy and the charge accumulation powers are based on electronegativity. Extended Huckel molecular orbital (EHMO) calculations were performed on the bimetallic cluster $[(R_3P)_{10}Au_{13}Ag_{12}Cl_7]^{2+}$ where R = H, in order to assess the electronic origins of the site preference principles. It is hoped that basic understanding of the principles governing site preference and alloy formation in multimetallic cluster systems will lead to better electronic and stereochemical controls of their structures and, ultimately, to the design and manufacture or fabrication of structurally well-defined multimetallic catalysts, ultrafine particles, nanoarchitectures, etc.

(I) Introduction

High-nuclearity mixed-metal clusters[1–4] are important in that they may serve as structurally well-defined models for multimetallic catalysts or nanoparticles. Our ongoing work in this area has given rise to a unique sequence of bimetallic (Au–Ag) clusters whose metal frameworks are based on *vertex-sharing polyicosahedra*.[5–9] We refer to these high-nuclearity mixed-metal clusters as "*clusters of clusters*".[5–7] This "*cluster of clusters*" series follows well-defined design rules, resulting in a novel *growth sequence* by successive additions of icosahedral units via vertex-sharing, as exemplified by the biicosahedral[8] $[(p\text{-}tol_3P)_{10}Au_{13}Ag_{12}Br_8]^+$,[8b] the triicosahedral[9] $[(p\text{-}tol_3P)_{12}Au_{18}Ag_{20}Cl_{14}]$,[9a] and the tetraicosahedral[9d] $[(Ph_3P)_{12}Au_{22}Ag_{24}Cl_{10}]$ clusters. The biicosahedral 25-metal-atom cluster series[8a–f] of general formula $[(R_3P)_{10}Au_{13}Ag_{12}X_8]^+$ (where R = phenyl or tolyl and X = Cl or Br) is particularly interesting in that they exhibit various metal configurations and bridging ligand arrangements caused by the relative rotations of the two metal icosahedra (about the shared

* Abstract published in *Advance ACS Abstracts*, July 15, 1994.

(1) For reviews, see, for example: (a) Shriver, D. F., Kaesz, H. D., Adams, R. D., Eds. *The Chemistry of Metal Cluster Complexes*, VCH Publishers: New York, 1990. (b) Johnson, B. F. G. Ed., *Transition Metal Clusters*; Wiley-Interscience: Chichester, England, 1980.

(2) (a) Whoolery, A. J.; Dahl, L. F. *J. Am. Chem. Soc.* **1991**, *113*, 6683. (b) Broach, R. W.; Dahl, L. F.; Longoni, G.; Chini, P.; Schultz, A. J.; Williams J. M. *Adv. Chem. Ser.* **1978**, *No. 167*, 93. (c) Elliott, G. P.; Howard, J. A. K.; Mise, T.; Nunn, C. M.; Stone, F. G. A. *Angew. Chem. Int. Ed. Engl.* **1986**, *25*, 190. (d) Smith, D. E.; Welch, A. J.; Treurnicht, I.; Puddephatt , R. J. *Inorg. Chem.* **1986**, *25*, 4616.

(3) (a) Braunstein, P.; Rose, J. In *Stereochem. Organomet. Inorg. Compounds*; Bernal, I., Ed.; Elsevier: Amsterdam, 1988; Vol. 3, p 320. (b) Gladfelter, W. L.; Geoffroy F. L. *Adv. Organomet. Chem.* **1980**, *18*, 207. (c) Amoroso, A. J.; Gade, L. H.; Johnson, B. F. G.; Lewis, J;.Raithby, P. R.; Wong. W.-T. *Angew. Chem., Int. Ed. Engl.* **1991**, *30*, 107.

(4) (a) Ceriotti, A.; Demartin, F.; Longoni, G.; Manassero, M.; Marchionna, M.; Piva, G.; Sansoni, M. *Angew. Chem. Int. Ed. Engl.* **1985**, *24*, 697. (b) Ceriotti, A.; Fait, A.; Longoni, G.; Piro, G. *J. Am. Chem. Soc.* **1986**, *108*, 8091. (c) Longoni, G.; Manassero, M.; Sansoni, M. *J. Am. Chem. Soc.* **1980**, *102*, 3242. (d) Fumagalli, A.; Martinengo, S.; Ciani, G.; Sironi, A. *J. Chem. Soc., Chem. Commun.* **1983**, 453.

(5) (a) Teo, B. K.; Zhang, H. *Proc. Natl. Acad. Sci. U.S.A.* **1991**, *88*, 5067. (b) Teo, B. K; Zhang, H.; Shi, X. In *The Chemistry of the Copper and Zinc Triads*; Welch, A. J., Chapman, S. K., Eds.; The Royal Society of Chemistry: London, 1993; pp 211–234.

(6) (a) Teo, B. K.; Zhang, H. *J. Cluster Sci.* **1990**, *1*, 223. (b) Teo, B. K.; Zhang, H. *J. Cluster Sci.* **1990**, *1*, 155. (c) Teo, B. K.; Zhang, H. *Polyhedron* **1990**, *9*, 1985. (d) Teo, B. K. *Polyhedron* **1988**, *7*, 2317.

(7) (a) Teo, B. K.; Zhang, H. *Inorg. Chem.* **1988**, *27*, 414. (b) Teo, B. K.; Zhang, H. *Inorg. Chim. Acta* **1988**, *144*, 173.

(8) (a) Teo, B. K.; Keating, K. *J. Am. Chem. Soc.* **1984**, *106*, 2224. (b) Teo, B. K.; Zhang, H.; Shi, X. *Inorg. Chem.* **1990**, *29*, 2083. (c) Teo, B. K.; Shi, X.; Zhang, H. *J. Am. Chem. Soc.* **1991**, *113*, 4329. (d) Teo, B. K.; Zhang, H. *Angew. Chem., Int. Ed. Engl.* **1992**, *31*, 445;. (e) Teo, B. K.; Shi, X.; Zhang, H. *J. Chem. Soc., Chem. Commun.* **1992**, 1195. (f) Teo, B. K.; Shi, X.; Zhang, H. *J. Cluster Sci.* **1993**, *4*, 471. (g) Teo, B. K.; Zhang, H. *Inorg. Chem.* **1991**, *30*, 3115.

(9) (a) Teo, B. K.; Zhang, H.; Shi, X. *J. Am. Chem. Soc.* **1990**, *112*, 8552. (b) Teo, B. K.; Hong, M.; Zhang, H.; Huang, D.; Shi, X. *J. Chem. Soc., Chem. Commun.* **1988**, 204. (c) Teo, B. K.; Hong, M.; Zhang, H.; Huang, D. *Angew. Chem., Int. Ed. Engl.* **1987**, *26*, 897. (d) Teo, B. K;.Shi, X.; Zhang, H. Cited in *Chem. Eng. News* **1989**, *67*, 6.

0020-1669/94/1333-4086$04.50/0

vertex) and the satellite ring of bridging ligands, respectively (as represented by the large circles and an ellipse in Chart 1, top figures). For example, the monocationic cluster $[(Ph_3P)_{10}Au_{13}Ag_{12}Br_8]^+$,[8c] with a staggered–eclipsed–staggered (*ses*) arrangement of four adjacent metal pentagons, has a ring of six bromides bridging the two middle silver pentagons. The dicationic cluster $[(p\text{-}tol_3P)_{10}Au_{13}Ag_{12}Cl_7]^{2+}$,[8g] however, with a nearly *ses* metal configuration, has five bridging halides.

Recently, we communicated a trimetallic cluster containing Au, Ag, and Pt, $[(Ph_3P)_{10}Au_{12}Ag_{12}PtCl_7]^+$ (**1**),[10] as the Cl^- salt. **1** represents the first example of a trimetallic polyicosahedral supracluster. Unfortunately, the location of the platinum atom in **1** cannot be ascertained because the X-ray scattering powers of Pt and Au are similar. For example, the unique platinum atom may occupy one of the two icosahedral centers or the shared vertex, as depicted in **2** and **3**, respectively. In order to resolve

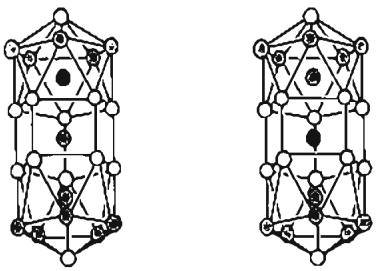

2 **3**

O/O/● = Au/Ag/M

this site preference, we have prepared and structurally characterized the Ni analog of **1**: the $[(Ph_3P)_{10}Au_{12}Ag_{12}NiCl_7]^+$ monocation (**4**), as the SbF_6^- salt, which is reported here for the first time. In **4**, the locality of the unique Ni atom can be unequivocably determined as a result of drastically different X-ray scattering powers of the three metallic constituents (Au, Ag, and Ni). **4** is the *first* Au–Ag–Ni compound ever reported.[2a] It is also the *first* example of a polyicosahedral structure containing first, second, and third row transition metals; as such it opens the door to other trimetallic polyicosahedral clusters containing Au, Ag, and Ni. Prior to this work, our work on polyicosahedral clusters involved only combinations of second and third row transition metals; hence, **4** represents the first example in which a first row transition metal is incorporated into a polyicosahedral cluster.

The title clusters are important in the elucidation of site preference in vertex-sharing polyicosahedral clusters containing group 10 and 11 metals. Such structural and bonding information are crucial in order to understand alloy formation in materials such as multimetallic catalysts, nanoparticles,[12] thin films, etc. Understanding of such alloy formation will allow better electronic and stereochemical controls of their structures and hence improve the design and manufacture of these materials (e.g., preparation of structurally well-defined catalysts[11] with tailor-made reactivities and selectivities or fabrication of quantum devices[12] with specific functions).

Chart 1

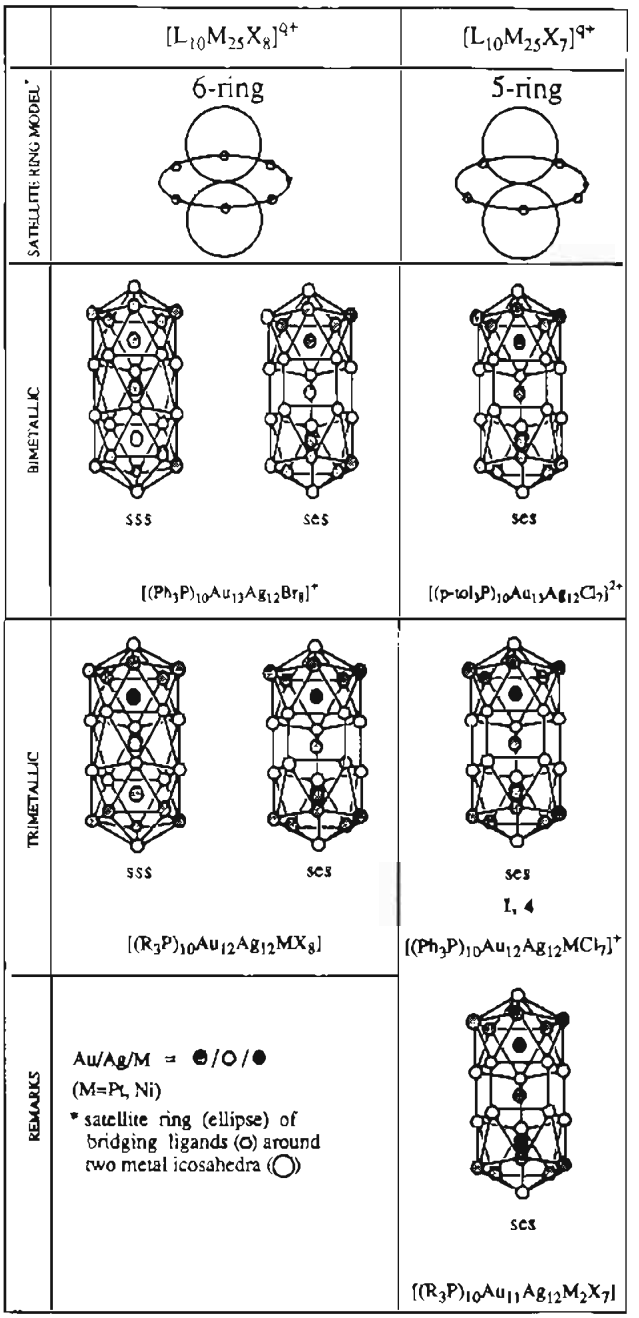

In this paper, we report the syntheses and structures of the title clusters **1** and **4**. On the basis of these structures, a set of site preference rules are deduced and compared with the corresponding bimetallic bicosahedral series. Extended Huckel molecular orbital (EHMO) calculations were performed on the bimetallic cluster $[(R_3P)_{10}Au_{13}Ag_{12}Cl_7]^{2+}$ where R = H, in order to assess the electronic origins of the site preference principles. These site preference principles and their bonding implications, are rationalized via simple bond strength vs charge accumulation (BSCA) plots. We note that these structural and bonding principles are applicable to other multimetallic systems, even though the terminologies may be different in different technologies. For example, terms such as site preference, interstitial vs surface sites in metallic clusters are equivalent to terms such as segregation (surface enrichment) and interior (kernel) vs exterior (mantle) often used in metal catalysts or particles.

(II) Experimetal Section

(A) Syntheses and Characterizations. **$[(Ph_3P)_{10}Au_{12}Ag_{12}PtCl_7]^+Cl^-$ (1(Cl)).** **1**, as the Cl^- salt, was prepared by reducing a mixture of $[(Ph_3P)_8$-

(10) Teo, B. K.; Zhang, H.; Shi, X. *J. Am. Chem. Soc.* **1993**, *115*, 8489.

(11) (a) Sachtler, W. M. H.; van Santen, R. A. *Adv. Catal.* **1977**, *26*, 69. (b) Sinfelt, J. H. *Bimetallic Catalysts: Discoveries, Concepts, and Applications*; J. Wiley & Sons: New York, 1983; pp 1–164 and references cited therein. (c) Gates, B. C.; Guczi, L.; Knozinger, H. *Metal Clusters in Catalysis*; Elsevier: Amsterdam, 1988. (d) Whitmire, K. H. *J. Coord. Chem.* **1988**, *17*, 95. (e) Boudart, M. *Adv. Catal.* **1969**, *20*, 153. (f) Boudart, M. *J. Mol Catal.* **1985**, *30*, 27.

(12) (a) Stucky, G. D.; Herron, N.; Wang, Y.; Eddy, M.; Cox, D.; Moller, K.; Bein, T. *J. Am. Chem. Soc.* **1989**, *111*, 530. (b) Stucky, G. D.; MacDougall, J. E.; Eckert, H.; Herron, N.; Wang, Y.; Moller, K.; Bein, T. *J. Am. Chem. Soc.* **1989**, *111*, 8006.

Table 1. Summary of Crystal Data, Collection and Reduction of X-ray Data, and Solution and Refinement of Structures

(a) $[(Ph_3P)_{10}Au_{12}Ag_{12}PtCl_7]Cl\cdot 17C_2H_5OH$		(b) $[(Ph_3P)_{10}Au_{12}Ag_{12}NiCl_7]SbF_6\cdot 15C_2H_5OH$	
A. Crystal Data		**A. Crystal Data**	
formula	$[(Ph_3P)_{10}Au_{12}Ag_{12}PtCl_7]Cl$	formula	$[(Ph_3P)_{10}Au_{12}Ag_{12}NiCl_7]SbF_6$
cryst color	dark-brown	cryst color	dark-red
cryst shape	paralleleoiped	cryst shape	parallelepiped
cryst size, mm³	0.18 × 0.16 × 0.12	cryst size, mm³	0.14 × 0.10 × 0.08
cell params (errors)		cell params (errors)	
a, Å	16.534(3)	*a*, Å	16.591(4)
b, Å	24.360(4)	*b*, Å	23.707(3)
c, Å	29.819(6)	*c*, Å	29.954(5)
β, deg	103.25(3)	β, deg	103.31(3)
cell vol, Å³	11690.3	cell vol, Å³	11465.2
Z	2	*Z*	2
Laue symmetry	monoclinic	Laue symmetry	monoclinic
space group	$P2_1/m$	space group	$P2_1/m$
syst absences	$0k0, k = 2n + 1$	syst absences	$0k0, k = 2n + 1$
equiv positions	$\pm(x, y, z)$	equiv positions	$\pm(x, y, z)$
	$\pm(x, {}^1/_2 - y, z)$		$\pm(x, {}^1/_2 - y, z)$
B. Collection and Reduction of X-ray Diffraction Data		**B. Collection and Reduction of X-ray Diffraction Data**	
diffractometer	Enraf-Nonius CAD4	diffractometer	Enraf-Nonius CAD4
radiation	Mo Kα	radiation	Mo Kα
wavelength, Å	0.7107	wavelength, Å	0.7107
temp, °C	23 ± 2	temp, °C	23 ± 2
scan technique	$\omega/2\theta$	scan technique	$\omega/2\theta$
scan rate (limits) deg/min	4–16	scan rate (limits) deg/min	4–16
scan range, deg	$(0.60 + 0.35 \tan\theta)$	scan range, deg	$(0.60 + 0.35 \tan\theta)$
no./freq of std reflcns	3/200	no./freq of std reflcns	3/200
2θ limits, deg	$2 < 2\theta < 45$	2θ limits, deg	$2 < 2\theta < 44$
cutoff of obsd data	$3\sigma(I)$	cutoff of obsd data	$3\sigma(I)$
no. of unique data[a]	3014	no. of unique data[a]	1822
octant	$\pm h,+k,+l$	octant	$\pm h,k,l$
linear abs coeff, cm⁻¹	92.6	linear abs coeff, cm⁻¹	89.8
abs cor	no	abs cor	ψ scan
C. Solution and Refinement		**C. Solution and Refinement**	
technique of solution	direct methods	technique of solution	direct methods
method of refinement	full-matrix least squares[b]	method of refinement	full-matrix least squares[b]
std dev	full variance–covariance	std dev	full variance–covariance
anisotropic convergence[c]	$R_1 = 7.0\%$, $R_2 = 8.5\%$	anisotropic convergence[c]	$R_1 = 6.9\%$, $R_2 = 8.8\%$
max shifts (Δ/σ)	0.75	max shifts (Δ/σ)	0.87
data/param	3014/205	data/param	1822/205
max residual intens of final diff map, e/Å³	<1.0	max residual intens of final diff map, e/Å³	<1.0

[a] The raw intensity is given as $I_{raw} = (20.116 \times ATN) \times (C - R \times B)/NPI$; here C = total counts, R = ratio of scan time to background counting time, B = total background counts, NPI = ratio of fastest possible scan rate to scan rate for the measurement, and ATN = attenuator factor (10.7 for Mo in our case). And the observed structure factor amplitude is obtained as the square root of the intensity after correction for Lorentz–polarization: $F_{obs} = (I_{raw}/Lp)^{1/2}$. [b] All least-squares refinements were based on the minimizations of $\sum w_i||F_o| - |F_c||^2$ with the individual weights $w_i = 1/\sigma(F_o)^2$. Atomic scattering factors used for all atoms are from: Cromer, D. T.; Waber, J. T. *International Tables for X-ray Crystallography*; The Kynoch Press: Birmingham, England, 1974; Vol. IV, Table 2.2B. Cromer, D. T.; Mann, J. B. X-ray Scattering Factors Computed From Numerical Hartree-Fock Wave Functions. *Acta Crystallogr.* **1968**, *A24*, 321–324. [c] $R_1 = [\sum||F_o| - |F_c||/\sum|F_o|] \times 100\%$ and $R_2 = [\sum w_i||F_o| - |F_c||^2/\sum w_i|F_o|^2]^{1/2} \times 100\%$.

$Au_8Pt](NO_3)_2$[13] (28 mg) and $(Ph_3P)_4Ag_4Cl_4$[14] (32 mg) with $NaBH_4$ (4 mg) in 30 mL of absolute ethanol. The color of the solution turned dark brown immediately upon addition of the reducing reagent. The reaction mixture was allowed to stir overnight and filtered. The resulting dark brown-red precipitate was washed with 5 mL of ethanol and 10 mL of diethyl ether and redissolved in dichloromethane and filtered again to get rid of insoluble impurities. The filtrate was then evaporated to dryness and recrystallized from $CH_2Cl_2/CH_3CN/C_2H_5OH$. Yield: 18 mg (37%, based on Pt). Crystals (parallelepiped shape) suitable for X-ray diffraction studies were grown from $CH_2Cl_2/CH_3CN/C_2H_5OH$ (in approximately 1:1:1 ratio) via evaporation. X-ray fluorescence analysis on the single crystals confirmed the presence of Pt, Au, Ag, and Cl atoms. IR showed the presence of metal-coordinated Ph_3P and the absence of NO_3^-.

$[(Ph_3P)_{10}Au_{12}Ag_{12}NiCl_7]^+(SbF_6)^-$ ($4(SbF_6)$). **4**, as the SbF_6^- salt, was similarly prepared by reducing a mixture of $[(Ph_3P)_8Au_8Ni](NO_3)_2$[15] (39 mg) and $(Ph_3P)_4Ag_4Cl_4$[14] (32 mg) with $NaBH_4$ (4 mg) in 40 mL of absolute ethanol except that $NaSbF_6$ (26 mg) was added to the ethanol filtrate and that the final product was recrystallized from CH_2Cl_2/EtOH. Yield: 26 mg (38%, based on Ni). Crystals (parallelepiped shape) suitable for X-ray diffraction studies were grown from CH_2Cl_2/EtOH (5:1 ratio) via evaporation. X-ray fluorescence analysis on the single crystals confirmed the presence of Ni, Au, Ag, and Cl atoms. IR showed the presence of metal-coordinated Ph_3P and the presence of SbF_6^-.

(B) Collection and Reduction of X-ray Data. A dark-brown parallelepiped shape crystal of **1**(Cl), with dimensions 0.18 mm × 0.16 mm × 0.12 mm, and a dark-red parallelepiped-shaped crystal of **4**(SbF_6), with dimensions 0.14 mm × 0.10 mm × 0.08 mm, were selected and mounted in the capillary tube with the mother liquor. Room-temperature (23 ± 2 °C) single-crystal X-ray diffraction data ($2 < \theta < 45°$) were collected on an Enraf-Nonius CAD4 diffractometer using graphite-monochromatized Mo Kα radiation (λ = 0.7107 Å). The observed intensities were corrected for Lorentz and polarization effects. Details of the crystal parameters and data collection are summarized in Table 1. A Wilson plot of the data favored the centrosymmetric space group $P2_1/m$ (No. 11). This centrosymmetric space group was later confirmed by the successful solution and refinement of the structure. Attempts to refine the structures in the acentric subgroup $P2_1$ were unsuccessful due to correlation of parameters.

(C) Solution and Refinement of the Structure. The crystal structures of both title compounds **1** and **4** were solved by using the SDP package.[16] Positions of the metal atoms were obtained from direct methods, and the Cl and P atoms were located *via* Fourier syntheses. The phenyl carbon atoms, the anions, and the solvent atoms were revealed from subsequent difference Fourier syntheses.

In the final cycles of refinement, anisotropic thermal parameters were used for heavy atoms (Pt, Au, Ag, Cl, and P for **1**(Cl) and Ni, Au, Ag,

(13) Bour, J. J.; Kanters, R. P. F.; Schlebos, P. P. J.; Bosman, W. P.; Behm, H.; Beurskens, P. T.; Steggerda, J. J. *Recl. Trav. Chim. Pays-Bas* **1987**, *106*, 157.

(14) Teo, B. K.; Calabrese, J. C. *Inorg. Chem.* **1976**, *15*, 2467.

(15) $[(Ph_3P)_8Au_8Ni](NO_3)_2$ was prepared by reducing a mixture of Ph_3PAuNO_3 and $(Ph_3P)_4Ni$ (8:1 molar ratio) in CH_2Cl_2 with $NaBH_4$ under inert atmosphere.

(16) For crystallographic details, see ref 8b.

Table 2. Atomic Positional Parameters and Equivalent Isotropic Displacement Parameters and Their Estimated Standard Deviations for the Clusters

atom	*x*	*y*	*z*	*B*,[a] Å^2	atom	*x*	*y*	*z*	*B*,[a] Å^2
				(a) $[(Ph_3P)_{10}Au_{12}Ag_{12}PtCl_7]Cl$ (**1**)					
Au1	0.0932(2)	0.4086(2)	0.1856(1)	3.48(8)	Cl11	0.134(2)	0.577(1)	0.269(1)	7.7(9)
Au2	0.2656(2)	0.4163(2)	0.2354(1)	3.41(8)	Cl1	0.232(2)	0.250	0.135(1)	4.8(9)
Au3	0.2715(2)	0.4100(2)	0.3328(1)	3.42(8)	Cl2	0.421(2)	0.250	0.286(1)	6(1)
Au4	0.1033(2)	0.4092(2)	0.3434(1)	3.25(8)	Cl3	0.270(2)	0.250	0.419(1)	4.0(9)
Au5	–0.0086(2)	0.4091(2)	0.2527(1)	3.73(9)	Cl4	–0.055(2)	0.250	0.347(1)	6(1)
AP11	0.1472(2)	0.3659(2)	0.2698(1)	2.44(7)	Cl5	–0.094(2)	0.250	0.166(1)	6(1)
Au13	0.1494(3)	0.250	0.2696(2)	4.4(1)	P1	0.052(2)	0.445(1)	0.1129(8)	4.5(7)
Ag11	0.1414(4)	0.4794(3)	0.2706(3)	4.5(2)	P2	0.359(1)	0.465(1)	0.2068(8)	3.7(6)
Ag1	0.1890(4)	0.3114(3)	0.1947(2)	4.1(2)	P3	0.375(1)	0.445(1)	0.3920(9)	4.5(7)
Ag2	0.3006(3)	0.3129(3)	0.2823(2)	3.3(2)	P4	0.065(1)	0.446(1)	0.4050(8)	3.6(6)
Ag3	0.2063(4)	0.3093(3)	0.3536(2)	3.7(2)	P5	–0.142(1)	0.445(1)	0.2381(8)	5.4(8)
Ag4	0.0301(4)	0.3091(4)	0.3071(2)	3.8(2)	Cl	0.661(2)	0.750	0.357(1)	5(1)
Ag5	0.0192(4)	0.3099(3)	0.2090(2)	3.8(2)					
				(b) $[(Ph_3P)_{10}Au_{12}Ag_{12}NiCl_7]SbF_6$ (**4**)					
Au1	0.4091(3)	0.0878(3)	0.3138(2)	3.7(1)	Cl1	0.265(4)	0.250	0.362(2)	6(2)
Au2	0.2388(3)	0.0802(3)	0.2650(2)	3.9(1)	Cl2	0.083(2)	0.250	0.218(1)	3(1)
Au3	0.2308(3)	0.0862(3)	0.1674(2)	3.8(1)	Cl3	0.222(4)	0.250	0.083(2)	7(2)
Au4	0.3988(3)	0.0875(3)	0.1572(2)	3.5(1)	Cl4	0.548(4)	0.250	0.148(2)	7(2)
Au5	0.5096(3)	0.0870(3)	0.2466(2)	4.2(1)	Cl5	0.601(4)	0.250	0.331(3)	10(2)
Au13	0.3527(5)	0.250	0.2312(3)	4.7(2)	Cl11	0.371(2)	–0.084(2)	0.230(1)	9(1)
AN11	0.3556(5)	0.1317(3)	0.2304(3)	1.8(2)	P1	0.451(2)	0.055(2)	0.387(1)	4(1)
Ag1	0.3143(6)	0.1876(6)	0.3047(4)	4.8(3)	P2	0.142(2)	0.029(1)	0.291(1)	3.3(9)
Ag2	0.2029(6)	0.1860(5)	0.2174(3)	3.9(3)	P3	0.132(2)	0.052(1)	0.111(1)	3.2(9)
Ag3	0.2970(6)	0.1894(6)	0.1470(4)	4.5(3)	P4	0.438(2)	0.054(2)	0.094(1)	3.6(9)
Ag4	0.4717(5)	0.1890(5)	0.1940(3)	3.9(3)	P5	0.644(2)	0.052(2)	0.263(1)	5(1)
Ag5	0.4840(6)	0.1881(5)	0.2904(3)	3.4(2)	Sb	0.156(1)	0.250	0.8623(7)	7.7(6)
Ag11	0.3600(6)	0.0149(4)	0.2299(4)	4.5(3)					

[a] Values for anisotropically refined atoms are given in the form of the isotropic equivalent displacement parameter defined as: $(4/3)\,[a^2B(1,1) + b^2B(2,2) + c^2B(3,3) + ab(\cos\gamma)B(1,2) + ac(\cos\beta)B(1,3) + bc(\cos\alpha)B(2,3)]$.

Cl, P, and Sb for **4**(SbF_6)), and all phenyl groups were refined using the rigid-body constraint as described previously.[9a] The occupancies of the solvent atoms were obtained by refining their multiplicities with a fixed isotropic thermal parameter of 8 Å^2. Subsequently, the solvent atoms were refined isotropically (at fixed multiplicities). Due to the liquidlike nature of the solvent molecules, no attempts were made to assign individual solvent atoms to solvent molecules or to differentiate between ethanol and acetonitrile. Final $R_1 = [\sum(|F_o| - |F_c|)/|F_o|] \times 100\%$ and $R_2 = [\sum w(|F_o| - |F_c|)^2/\sum w|F_o|^2]^{1/2}$ values were 7.0% and 8.5% for 3014 unique reflections with $I > 3\sigma(I)$ for **1**(Cl) and 6.9% and 8.8% for 1822 unique reflections with $I > 3\sigma(I)$ for **4**(SbF_6), respectively. The final difference map showed no peaks greater than 1.0 e/Å^3 except those close (<1.5 Å) to the heavy atoms. Final atomic coordinates and thermal parameters with the estimated standard deviations are presented in Tables 2, and A (supplementary material), respectively. The phenyl groups are numbered as PhiA, PhiB, and PhiC, indicating that the rings A, B, and C are bonded to the *i*th phosphine, respectively. The final positional and thermal parameters for each group (x, y, z, ϕ, θ, ρ, and B) are listed in Table B of the supplementary material. The final positional and thermal parameters of the solvent atoms are summarized in Table C of the supplementary material. Selected interatomic distances and bond angles, together with the estimated standard deviations, are given in Tables 3 and 4, respectively.

(III) Results and Discussion

(A) Description of the Structures. Parts a and b of Figure 1 depict the $Au_{12}Ag_{12}Pt$ core and $[P_{10}Au_{12}Ag_{12}PtCl_7]$ framework of **1**, whereas parts a and b of Figure 2 portray the $Au_{12}Ag_{12}Ni$ core and $[P_{10}Au_{12}Ag_{12}NiCl_7]$ framework of **4**, respectively. Under space group $P2_1/m$, each cluster conforms to crystallographic C_s–m site symmetry (with the mirror plane passing through Au13 and Cl1–Cl5). Consequently, the metal core of an individual cluster can be described as two Au_6Ag_6 icosahedra, one M-centered (M = Pt, Ni) and one Au-centered, sharing a common Au atom, as depicted schematically in **2**. The crystallographically imposed mirror plane symmetry necessitates a crystal-disorder of the M center (M = Pt (**1**), Ni (**4**)) and the Au center, designated as AP11 and AN11 in Figure 1a and Figure 2a, respectively, each representing an equal admixture of Au and M (M = Pt, Ni).[17] The arrangement of the four metal pentagons has an exact *ses* (staggered–eclipsed–staggered) configuration. The 10 Ph_3P groups coordinate to 10 peripheral Au atoms in a radial fashion. Of the seven chloride ligands, five are doubly bridging (Cl1–Cl5) which symmetrically connect the two middle Ag_5 pentagons (Figures 1c and 2c) and two are terminal (Cl11 and Cl11′) which coordinate to the two apical Ag atoms (Ag11 and Ag11′).

In comparison with the bimetallic (Au–Ag) biicosahedral clusters,[8] the most significant structural feature of **1** and **4** is that one of the two icosahedral centers in an individual cluster is occupied by the unique M = Pt (**1**) or Ni (**4**) atom (instead of Au) as depicted in **2**. In fact, one of the motivations of the present work was to determine whether the M atom (M = Pt, Ni) is either at one of the two icosahedral centers, or at the shared vertex, as illustrated schematically in **2** and **3**, respectively. In **1**,[10] the location of the unique platinum atom (i.e., **2** or **3**) cannot be discerned with certainty due to the similar X-ray scattering power of Pt and Au.[18] In **4**, on the other hand, the location of the unique Ni atom can be determined unambiguously owing to very different X-ray scattering powers[17] of the three metallic constituents (Au, Ag, and Ni). Hence, the structure of **4** unequivocably establishes the *site preference* for the group 10 metals (to be at the center(s) of the icosahedra, as in **2**, rather than at the shared vertex, as in **3**, in a polyicosahedral cluster containing both group 10 and group 11 metals.

(17) This crystal-disorder model is based on the marked differences in X-ray scattering power of Au, Ag, and Ni. The fact that the refined equivalent isotropic temperature factor of 1.8(2) Å^2 for AN11 and AN11′ (an equal admixture of Au and Ni) is less than the average value of 3.8(1) Å^2 for Au1 to Au5 is in complete accord with corresponding equivalent isotropic temperature factors observed for other vertex-sharing biicosahedral supraclusters in which the centers of icosahedra tend to have significantly smaller temperature factors. Refinements under $P2_1/m$ symmetry of the centroids of the two icosahedra either as pure Au or as pure Ni led to unreasonable temperature factors (B) of 7.0 and –3.5 Å^2, respectively.

(18) Since the publication of ref 10 and the submission of this paper, a related cluster $[(Ph_3P)_{10}Au_{10}Ag_{13}Pt_2Cl_7]$ has appeared: (Kappen, T. G. M. M.; Schlebos, P. P. J.; Bour, J. J.; Bosman, W. P.; Smits, J. M. M.; Beurskens, P. T.; Steggerda, J. J. *Inorg. Chem.* **1994**, *33*, 754. This latter cluster has the same problem as **1** in that Pt and Au cannot be distinguished crystallographically.

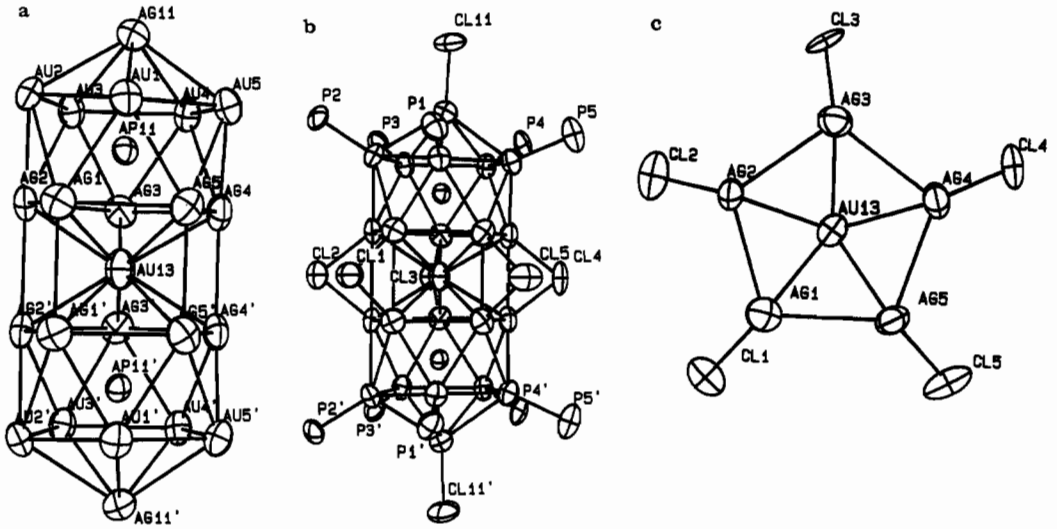

Figure 1. Molecular architecture of the 25-metal-atom cluster $[(Ph_3P)_{10}Au_{12}Ag_{12}PtCl_7]^+$ (**1**), as the Cl^- salt: (a) the metal core, $Au_{12}Ag_{12}Pt$; (b) the metal–ligand framework, $P_{10}Au_{12}Ag_{12}PtCl_7$; (c) projection of the two silver pentagons onto the crystallographic mirror which passes through Au13 and the five doubly bridging chloride ligands Cl1–Cl5. With the exception of AP11 and AP11′, the entire monocation (including the triphenylphosphine and the halide ligands) conforms to crystallographically imposed C_s–m site symmetry. Atoms related by the mirror symmetry are designated as primes. All radial bonds (12 each) from AP11 and AP11′ have been omitted for clarity. Some important distances are as follows (Å): AP11–Au(n), 2.687 (average); AP11–Ag(n), 2.810 (average); AP11–Ag11, 2.767(2); AP11–Au13, 2.824(7); Au13–Ag(n), 2.873 (average); intrapentagonal, Au(n)–Au(n + 1), 2.888 (average); Ag(n)–Ag(n + 1), 2.898 (average); interpentagonal, Ag(n)–Ag(n'), 2.949 (average) where n = 1–5; Au–P, 2.30 (average); Ag11–Cl11, 2.389(5); Ag(n)–Cl(n), 2.50 (average) where n = 1–5. The five doubly bridging chloride ligands form a slightly distorted pentagon with nonbonding distances (Å) of Cl1···Cl2, 4.87; Cl2···Cl3, 5.15; Cl3···Cl4, 5.31; Cl4···Cl5, 5.28; and Cl1···Cl5, 5.69.

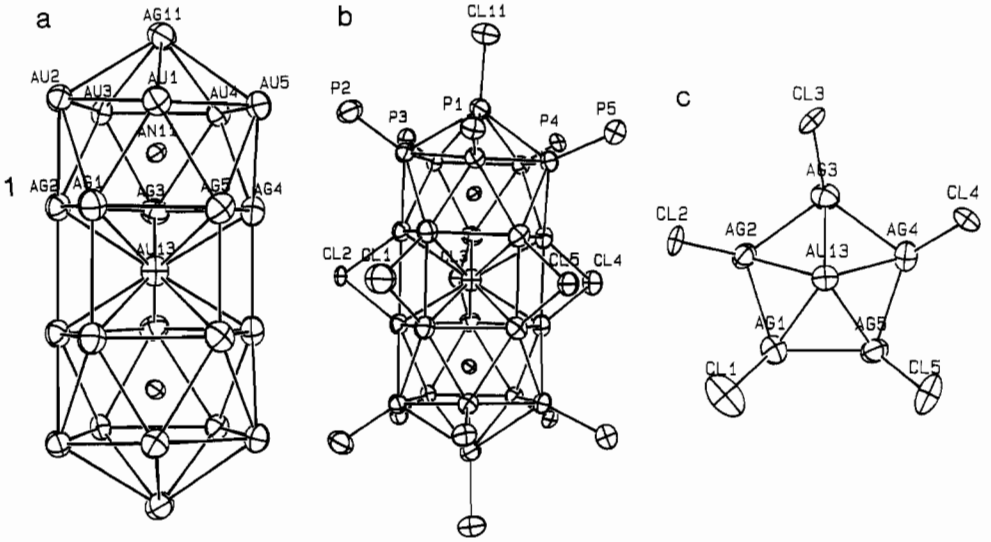

Figure 2. Molecular architecture of the 25-metal-atom cluster $[(Ph_3P)_{10}Au_{12}Ag_{12}NiCl_7]^+$ (**4**), as the SbF_6^- salt: (a) the metal core, $Au_{12}Ag_{12}Ni$; (b) the metal–ligand framework, $P_{10}Au_{12}Ag_{12}NiCl_7$; (c) projection of the two silver pentagons onto the crystallographic mirror which passes through Au13 and the five doubly bridging chloride ligands Cl1–Cl5. Atoms AN11 and AN11′ (centers of icosahedra) represent an equal admixture of Au and Ni due to the crystallographically imposed mirror (C_s–m) symmetry. With the exception of AN11 and AN11′, the entire monocation (including the triphenylphosphine and the halide ligands) conforms to crystallographically imposed C_s–m site symmetry. Atoms related by the mirror symmetry are not labeled. All radial bonds (12 each) from AN11 and AN11′ have been omitted for clarity. Some important distances are as follows (Å): AN11–Au(n), 2.683 (average); AN11–Ag(n), 2.80 (average); AN11–Ag11, 2.77(1); AN11–Au13, 2.806(8); Au13–Ag(n), 2.86 (average); intrapentagonal, Au(n)–Au(n + 1), 2.884 (average); Ag(n)–Ag(n + 1), 2.89 (average); interpentagonal, Ag(n)–Ag(n'), 2.94 (average) where n = 1–5; Au–P, 2.28 (average); Ag11–Cl11, 2.35(5); Ag(n)–Cl(n), 2.52 (average) where n = 1–5. The five doubly bridging chloride ligands form a slightly distorted pentagon with nonbonding distances (Å) of Cl1···Cl2, 4.67; Cl2···Cl3, 5.10; Cl3···Cl4, 5.31; Cl4···Cl5, 5.34; and Cl1···Cl5, 5.87.

Several novel structural features of **1** and **4** are noteworthy. First, the most significant structural characteristic is that one of the two icosahedral centers is occupied by the unique group 10 metal atom. Second, the shared vertex is Au as in the majority of the biicosahedral Au–Ag supraclusters.[8] Third, the observed metal configuration is exactly *ses* instead of nearly *ses* as in $[p\text{-tol}_3P_{10}Au_{13}Ag_{12}Cl_7]^{2+}$ (**5**).[8g] Fourth, there are *five* symmetrical-bridging chloride ligands in **1** and **4** instead of *six*, as in $[(Ph_3P)_{10}Au_{13}Ag_{12}Br_8]^+$ (**6**).[8c] Finally, while **6** is a *monocation* and **5** is a *dication*, the two title clusters, **1** and **4**, with a group 10 metal atom replacing one of the Au atoms, are *monocations* (vide infra).

(B) The Ubiquitous $P2_1/m$ Crystal Structure. Under the $P2_1/m$ space group, both the cationic clusters and the counteranions in **1** and **4** are located on the crystallographic mirror (m) planes. The centroids of the clusters (Au13) have fractional coordinates of (0.15, 0.25, 0.27) while the anions (Cl^- in **1** and SbF_6^- in **4**) are at, approximately, (0.66, 0.75, 0.36) (note that the choices of origin of the two title structures differ by ($^1/_2$, $^1/_2$, $^1/_2$)). Crystallographically, it is interesting to note that, despite the difference in the counteranions (Cl^- in **1** vs SbF_6^- in **4**), the two title clusters **1** and **4** are isomorphous and isostructural with similar molecular parameters. Even more surprising is the fact that both **1** and **4** are isomorphous, though not isostructural, with

Table 3. Selected Interatomic Distances (Å) and Their Estimated Standard Deviations for the Clusters[a]

(a) $[(Ph_3P)_{10}Au_{12}Ag_{12}PtCl_7]Cl$ (1)

Au1–Au2	2.887(4)	Au4–Ag4	2.825(9)	Au4–Ag3	2.946(9)	Ag1–Ag5	2.93(1)
Au1–Au5	2.895(5)	Au5–AP11	2.720(5)	Ag2–Ag3	2.91(1)	P2–Au2	2.28(3)
Au1–AP11	2.675(5)	Au5–Ag11	2.960(8)	Ag3–Ag4	2.925(8)	P2–C2A1	1.82(2)
Au1–Ag11	3.018(8)	Au5–Ag4	2.915(9)	Ag4–Ag5	2.890(9)	P2–C2B1	1.95(3)
Au1–Ag1	2.827(9)	Au5–Ag5	2.833(9)	Ag1–Ag1′	2.99(1)	P2–C2C1	1.94(2)
Au1–Ag5	2.854(9)	AP11–Au13	2.824(4)	Cl1–Ag1	2.55(3)	P3–Au3	2.32(2)
Au2–Au3	2.885(5)	AP11–Ag11	2.767(8)	Ag2–Ag2′	3.06(1)	P3–C3A1	1.78(3)
Au2–AP11	2.691(5)	AP11–Ag1	2.823(8)	Cl2–Ag2	2.50(3)	P3–C3B1	1.76(2)
Au2–Ag11	2.932(9)	AP11–Ag2	2.794(7)	Ag3–Ag3′	2.89(1)	P3–C3C1	1.75(3)
Au2–Ag1	2.977(9)	AP11–Ag3	2.823(7)	Cl3–Ag3	2.47(2)	P4–Au4	2.26(3)
Au2–Ag2	2.875(8)	AP11–Ag4	2.807(8)	Ag4–Ag4′	2.88(1)	P4–C4A1	1.87(2)
Au3–Au4	2.870(5)	AP11–Ag5	2.805(7)	Cl4–Ag4	2.49(3)	P4–C4B1	1.79(3)
Au3–AP11	2.672(4)	Au13–Ag1	2.885(9)	Ag5–Ag5′	2.92(1)	P4–C4C1	1.91(2)
Au3–Ag11	3.017(8)	Au13–Ag2	2.884(8)	Cl5–Ag5	2.49(3)	P5–Au5	2.32(3)
Au3–Ag2	2.903(9)	Au13–Ag3	2.858(8)	P1–Au1	2.29(2)	P5–C5A1	1.85(3)
Au3–Ag3	2.804(9)	Au13–Ag4	2.867(9)	P1–C1A1	1.79(3)	P5–C5B1	1.86(2)
Au4–Au5	2.904(4)	Au13–Ag5	2.869(8)	P1–C1B1	1.80(3)	P5–C5C1	1.76(3)
Au4–AP11	2.679(5)	Ag11–Cl11	2.39(3)	P1–C1C1	1.75(3)		
Au4–Ag11	2.942(9)	Ag1–Ag2	2.830(8)				

(b) $[(Ph_3P)_{10}Au_{12}Ag_{12}NiCl_7]SbF_6$ (4)

Au1–Au2	2.873(7)	Au4–Ag11	2.96(1)	Au3–P3	2.21(3)	Ag1–Ag5	2.94(1)
Au1–Au5	2.896(8)	Au4–P4	2.29(4)	Au4–Au5	2.878(7)	Ag1–Cl1	2.55(5)
Au1–AN11	2.664(9)	Au5–AN11	2.704(9)	Au4–AN11	2.67(1)	Ag2–Ag3	2.90(2)
Au1–Ag1	2.82(1)	Au5–Ag4	2.88(1)	Au4–Ag3	2.92(1)	Ag3–Ag4	2.92(1)
Au1–Ag5	2.85(1)	Au5–Ag5	2.81(1)	Au4–Ag4	2.80(1)	Ag4–Ag5	2.85(1)
Au1–Ag11	3.00(1)	Au5–Ag11	2.96(1)	Ag2–Cl2	2.50(3)	Ag5–Cl5	2.51(5)
Au1–P1	2.27(3)	Au5–P5	2.33(4)	Ag3–Cl3	2.49(5)	Ag1–Ag1′	2.96(2)
Au2–Au3	2.898(8)	Au13–AN11	2.806(8)	Ag4–Cl4	2.53(6)	Ag2–Ag2′	3.03(2)
Au2–AN11	2.69(1)	Au13–Ag1	2.84(1)	Ag11–Cl11	2.35(5)	Ag3–Ag3′	2.87(2)
Au2–Ag1	2.96(1)	Au13–Ag2	2.86(1)	P1–C1B1	1.75(4)	Ag4–Ag4′	2.89(2)
Au2–Ag2	2.88(1)	Au13–Ag3	2.86(1)	P2–C2A1	1.82(3)	Ag5–Ag5′	2.93(2)
Au2–Ag11	2.92(1)	Au13–Ag4	2.87(1)	P2–C2C1	1.70(3)	P1–C1A1	1.84(3)
Au2–P2	2.30(4)	Au13–Ag5	2.88(1)	P3–C3B1	1.71(3)	P1–C1C1	1.80(4)
Au3–Au4	2.874(7)	AN11–Ag1	2.81(1)	P4–C4A1	1.71(4)	P2–C2B1	1.87(4)
Au3–AN11	2.685(9)	AN11–Ag2	2.79(1)	P4–C4C1	1.86(3)	P3–C3A1	2.02(3)
Au3–Ag2	2.89(1)	AN11–Ag3	2.82(1)	P5–C5B1	1.85(4)	P3–C3C1	1.95(4)
Au3–Ag3	2.81(1)	AN11–Ag4	2.78(1)	Sb–F1	2.012(3)	P4–C4B1	1.99(4)
Au3–Ag11	3.02(1)	AN11–Ag5	2.79(1)	Sb–F5	1.63(2)	P5–C5A1	1.75(4)
Sb–F3	1.79(2)	Sb–F4	1.86(2)	AN11–Ag11	2.77(1)	P5–C5C1	1.81(3)
				Ag1–Ag2	2.83(1)	Sb–F2	1.63(2)

[a] Numbers in parentheses are estimated standard deviations in the least significant digits.

$[(Ph_3P)_{10}Au_{13}Ag_{12}X_8]^+$, as SbF_6 salt, where X = Cl,[8f] Br.[8c] In the latter clusters, there are six (instead of five) bridging halide ligands in the equatorial plane of the cluster. The ubiquity of the space group $P2_1/m$ (with cell parameters of, roughly, 16, 24, and 30 Å and $\beta = 103°$) for the series of vertex-sharing biicosahedral supraclusters with triphenylphosphine as ligands, regardless of the types of counteranions (e.g., SbF_6^- vs Cl^-), halide ligands (e.g., Cl^- vs Br^-), or solvent molecules, is rather interesting. We believe that this is attributable to three important factors (among others). First, the large metal clusters, with triphenylphosphines as a sheathing, pack in a similar fashion in space group $P2_1/m$, regardless of the type(s) of metal atoms (Pt, Ni, Au, Ag, etc) in the metal core. Second, a detailed examination of the surface of the clusters revealed that there are "corridors" along the idealized 5-fold axis of the cluster as well as "cracks" in the equatorial plane. These are the localities where the terminal and bridging halide ligands are situated (or buried). Hence, the crystal structure is more or less independent of the size (Cl vs Br) or the number (five or six), of the bridging halide ligands. Third, the sheer size of the metal cluster, in comparison to the solvent molecules or the counteranions, dictates the crystal packing and the crystal symmetry. The much smaller solvent molecules or the counteranions then occupy the intercluster voids. As a result, the crystal lattice is more or less indifferent to the solvent molecules and/or the anions.

In the above discussion, we assume that there are 10 triphenylphosphines coordinated to the 10 gold atoms in a way similar to that observed in the title clusters. Also implicit in the discussion is the assumption that the bonding and stereochemistry of the metal cores (with *ses* configuration) are similar even though the metal or halide ligand types or individual molecular parameters may vary. Substantial deviations from these assumptions will alter the crystal structure and symmetry. One obvious example is the observed cluster isomerization of $[(Ph_3P)_{10}Au_{13}Ag_{12}Br_8]^+$ from the *ses* to the *sss* metal configuration which results in a change of the crystal symmetry from $P2_1/m$ (as the SbF_6^- salt)[8c] to $C2/c$ (as the Br^- salt)[8e] with different cell parameters.

(C) Site Preference in Mixed-Metal Vertex-Sharing Polyicosahedral Clusters. Site preference is of prime importance in the understanding of structures and reactivities of mixed-metal clusters which may serve as structurally well-defined models for heterometallic catalysts[11] or nanoparticles.[12] Site preference in mixed-metal clusters is a manisfestation of the various and often competing bonding effects. In the following discussions, we shall assume that thermodynamic factors outweigh kinetic pathways in dictating the site preference.

(1) Bimetallic Au–Ag Supraclusters. For the bimetallic polyicosahedral Au–Ag supraclusters,[8,9] six empirical structural rules have been established:[19] (1) the centers of the icosahedra are gold atoms, (2) the "shared" vertices are most likely to be gold atoms, (3) phosphine ligands prefer coordination with surface gold atoms, (4) silver atoms prefer surface sites, especially those at the boundary of neighboring icosahedra, (5) the capping atoms are most likely to be silver atoms, and (6) halide ligands prefer coordination with silver atoms. As pointed out previously,[19,20] these structural rules can be rationalized in terms of the disparities

(19) Teo, B. K.; Shi, X.; Zhang, H. *Inorg. Chem.* **1993**, *32*, 3987.
(20) Teo, B. K.; Zhang, H.; Kean, Y.; Dang, H.; Shi, X. *J. Chem. Phys.* **1993**, *99*, 2929.

Table 4. Bond Angles (deg) and Their Estimated Standard Deviations for the Clusters[a]

(a) $[(Ph_3P)_{10}Au_{12}Ag_{12}PtCl_7]Cl$ (**1**)

Au2–Au1–Au5	107.6(1)	AP11–Au4–P4	179.5(6)	Au13–AP11–Ag4	61.2(2)	Au3–Ag11–Cl11	126.8(7)
Au2–Au1–AP11	57.7(1)	AP11–Au4–Ag3	109.9(2)	Au13–AP11–Ag5	61.3(2)	Au4–Ag11–Au5	59.0(2)
Au2–Au1–Ag11	59.5(2)	Ag11–Au4–Ag4	111.4(2)	Ag11–AP11–Ag1	119.5(3)	Au4–Ag11–AP11	55.9(2)
Au2–Au1–Ag1	62.8(2)	Ag11–Au4–P4	120.9(7)	Ag11–AP11–Ag2	119.5(2)	Au4–Ag11–Cl11	125.0(9)
Au2–Au1–Ag5	110.7(2)	Ag3–Au4–Ag4	60.9(2)	Ag11–AP11–Ag3	119.1(2)	Au5–Ag11–AP11	56.6(2)
Au2–Au1–P1	120.3(7)	Ag3–Au4–P4	120.5(6)	Ag11–AP11–Ag4	117.4(3)	Au5–Ag11–Cl11	122.3(7)
Au5–Au1–AP11	58.3(1)	Ag4–Au4–P4	118.8(7)	Ag11–AP11–Ag5	118.0(2)	AP11–Ag11–Cl11	178.4(7)
Au5–Au1–Ag11	60.0(2)	Au1–Au5–Au4	107.2(1)	Ag1–AP11–Ag2	60.5(2)	Au1–Ag1–Au2	59.6(2)
Au5–Au1–Ag1	109.8(2)	Au1–Au5–AP11	56.8(1)	Ag1–AP11–Ag3	111.9(2)	Au1–Ag1–AP11	56.5(2)
Au5–Au1–Ag5	59.1(2)	Au1–Au5–Ag11	62.1(2)	Ag1–AP11–Ag4	113.5(3)	Au1–Ag1–Au13	106.6(3)
Au5–Au1–P1	123.9(7)	Au1–Au5–Ag4	107.0(2)	Ag1–AP11–Ag5	62.8(2)	Au1–Ag1–Ag1	146.9(3)
AP11–Au1–Ag11	57.8(2)	Au1–Au5–Ag5	59.8(2)	Ag2–AP11–Ag3	62.4(2)	Au–Ag1–Ag2	108.1(3)
AP11–Au1–Ag1	61.7(2)	Au1–Au5–P5	123.4(7)	Ag2–AP11–Ag4	114.0(2)	Au1–Ag1–Ag5	59.4(2)
AP11–Au1–Ag5	60.9(2)	Au4–Au5–AP11	56.8(1)	Ag2–AP11–Ag5	112.8(2)	Au1–Ag1–Cl1	131.6(6)
AP11–Au1–P1	177.7(7)	Au4–Au5–Ag11	60.2(2)	Ag3–AP11–Ag4	62.6(2)	Au2–Ag1–AP11	55.2(2)
Ag11–Au1–Ag1	111.4(2)	Au4–Au5–Ag4	58.1(2)	Ag3–AP11–Ag5	113.0(2)	Au2–Ag1–Au13	106.2(2)
Ag11–Au1–Ag5	108.8(2)	Au4–Au5–Ag5	107.1(2)	Ag4–AP11–Ag5	62.0(2)	Au2–Ag1–Ag1	149.1(3)
Ag11–Au1–P1	122.6(7)	Au4–Au5–P5	123.4(7)	AP11–Au13–AP11	178.5(3)	Au2–Ag1–Ag2	59.3(2)
Ag1–Au1–Ag5	62.2(2)	AP11–Au5–Ag11	58.1(2)	AP11–Au13–Ag1	59.3(2)	Au2–Ag1–Ag5	106.1(3)
Ag1–Au1–P1	116.7(7)	AP11–Au5–Ag4	59.7(2)	AP11–Au13–Ag1	121.7(3)	Au2–Ag1–Cl1	128.9(7)
Ag5–Au1–P1	120.1(7)	AP11–Au5–Ag5	60.6(2)	AP11–Au13–Ag2	58.6(2)	AP11–Ag1–Au13	59.3(2)
Au1–Au2–Au3	108.8(1)	AP11–Au5–P5	179(1)	AP11–Au13–Ag2	122.8(2)	AP11–Ag1–Ag1	118.1(3)
Au1–Au2–AP11	57.2(1)	Ag11–Au5–Ag4	108.4(2)	AP11–Au13–Ag3	59.6(2)	AP11–Ag1–Ag2	59.2(2)
Au1–Au2–Ag11	62.5(2)	Ag11–Au5–Ag5	111.0(2)	AP11–Au13–Ag3	120.3(2)	AP11–Ag1–Ag5	58.3(2)
Au1–Au2–Ag1	57.6(2)	Ag11–Au5–P5	122.4(8)	AP11–Au13–Ag4	59.1(2)	AP11–Ag1–Cl1	171.5(6)
Au1–Au2–Ag2	105.2(2)	Ag4–Au5–Ag5	60.4(2)	AP11–Au13–Ag4	119.4(3)	Au13–Ag1–Ag1	58.8(2)
Au1–Au2–P2	121.3(6)	Ag4–Au5–P5	119.9(8)	AP11–Au13–Ag5	59.0(2)	Au13–Ag1–Ag2	60.6(2)
Au3–Au2–AP11	57.1(1)	Ag5–Au5–P5	118.9(7)	AP11–Au13–Ag5	120.2(2)	Au13–Ag1–Ag5	59.1(2)
Au3–Au2–Ag11	62.5(2)	Au1–AP11–Au2	65.1(1)	AP11–Au13–Ag1	121.7(3)	Au13–Ag1–Cl1	112.8(6)
Au3–Au2–Ag1	106.3(2)	Au1–AP11–Au3	122.8(2)	AP11–Au13–Ag1	59.3(2)	Ag1–Ag1–Ag2	90.8(3)
Au3–Au2–Ag2	60.5(2)	Au1–AP11–Au4	121.4(2)	AP11–Au13–Ag2	122.8(2)	Ag1–Ag1–Ag5	89.3(3)
Au3–Au2–P2	122.1(6)	Au1–AP11–Au5	64.9(1)	AP11–Au13–Ag2	58.6(2)	Ag1–Ag1–Cl1	54.2(5)
AP11–Au2–Ag11	58.8(2)	Au1–AP11–Au13	112.8(2)	AP11–Au13–Ag3	120.3(2)	Ag2–Ag1–Ag5	108.0(3)
AP11–Au2–Ag1	59.5(2)	Au1–AP11–Ag11	67.3(2)	AP11–Au13–Ag3	59.6(2)	Ag2–Ag1–Cl1	115.1(7)
AP11–Au2–Ag2	60.2(2)	Au1–AP11–Ag1	61.8(2)	AP11–Au13–Ag4	119.4(3)	Ag5–Ag1–Cl1	121.7(7)
AP11–Au2–P2	175.7(7)	Au1–AP11–Ag2	113.7(2)	AP11–Au13–Ag4	59.1(2)	Au2–Ag2-Au3	59.9(2)
Ag11–Au2–Ag1	109.6(2)	Au1–AP11–Ag3	173.4(2)	AP11–Au13–Ag5	120.2(2)	Au2–Ag2–AP11	56.6(2)
Ag11–Au2–Ag2	111.7(2)	Au1–AP11–Ag4	116.8(2)	AP11–Au13–Ag5	59.0(2)	Au2–Ag2–Au13	109.0(2)
Ag11–Au2–P2	116.9(7)	Au1–AP11–Ag5	62.7(2)	Ag1–Au13–Ag1	62.4(3)	Au2–Ag2–Ag1	62.9(2)
Ag1–Au2–Ag2	57.8(2)	Au2–AP11–Au3	65.1(1)	Ag1–Au13–Ag2	58.8(2)	Au2–Ag2–Ag2	151.1(2)
Ag1–Au2–P2	123.7(7)	Au2–AP11–Au4	119.2(2)	Ag1–Au13–Ag2	91.9(3)	Au2–Ag2–Ag3	107.2(3)
Ag2–Au2–P2	123.7(6)	Au2–AP11–Au5	119.1(2)	Ag1–Au13–Ag3	109.2(2)	Au2–Ag2–Cl2	129.4(8)
Au2–Au3–Au4	107.1(1)	Au2–AP11–Au13	116.4(2)	Ag1–Au13–Ag3	148.4(3)	Au3–Ag2–AP11	55.9(2)
Au2–Au3–AP11	57.8(1)	Au2–AP11–Ag11	65.0(2)	Ag1–Au13–Ag4	109.9(2)	Au3–Ag2–Au13	105.0(2)
Au2–Au3–Ag11	59.5(2)	Au2–AP11–Ag1	65.3(2)	Ag1–Au13–Ag4	149.5(2)	Au3–Ag2–Ag1	109.8(3)
Au2–Au3–Ag2	59.6(2)	Au2–AP11–Ag2	63.2(2)	Ag1–Au13–Ag5	61.3(2)	Au3–Ag2–Ag2	144.5(3)
Au2–Au3–Ag3	109.9(2)	Au2–AP11–Ag3	115.2(2)	Ag1–Au13–Ag5	92.7(2)	Au3–Ag2–Ag3	57.7(2)
Au2–Au3–P3	126.8(7)	Au2–AP11–Ag4	177.2(2)	Ag2–Au13–Ag2	64.2(2)	Au3–Ag2–Cl2	134.4(7)
Au4–Au3–AP11	57.7(1)	Au2–AP11–Ag5	118.5(2)	Ag2–Au13–Ag3	60.9(2)	AP11–Ag2–Au13	59.6(1)
Au4–Au3–Ag11	59.9(2)	Au3–AP11–Au4	64.9(1)	Ag2–Au13–Ag3	92.9(2)	AP11–Ag2–Ag1	60.3(2)
Au4–Au3–Ag2	109.4(2)	Au3–AP11–Au5	121.3(2)	Ag2–Au13–Ag4	109.6(2)	AP11–Ag2–Ag2	117.5(2)
Au4–Au3–Ag3	62.5(2)	Au3–AP11–Au13	113.3(2)	Ag2–Au13–Ag4	150.3(3)	AP11–Ag2–Ag3	59.3(2)
Au4–Au3–P3	118.8(7)	Au3–AP11–Ag11	67.4(2)	Ag2–Au13–Ag5	108.3(2)	AP11–Ag2–Cl2	168.9(6)
AP11–Au3–Ag11	57.8(2)	Au3–AP11–Ag1	117.3(2)	Ag2–Au13–Ag5	148.8(3)	Au13–Ag2–Ag1	60.6(2)
AP11–Au3–Ag2	60.0(2)	Au3–AP11–Ag2	64.1(2)	Ag3–Au13–Ag3	60.7(2)	Au13–Ag2–Ag2	57.9(2)
AP11–Au3–Ag3	62.0(2)	Au3–AP11–Ag3	61.3(2)	Ag3–Au13–Ag4	61.4(2)	Au13–Ag2–Ag3	59.1(2)
AP11–Au3–P3	175.4(7)	Au3–AP11–Ag4	114.1(2)	Ag3–Au13–Ag4	91.7(3)	Au13–Ag2–Cl2	109.9(5)
Ag11–Au3–Ag2	108.5(2)	Au3–AP11–Ag5	174.2(2)	Ag3–Au13–Ag5	110.1(2)	Ag1–Ag2–Ag2	89.2(3)
Ag11–Au3–Ag3	111.7(2)	Au4–AP11–Au5	65.1(1)	Ag3–Au13–Ag5	149.1(3)	Ag1–Ag2–Ag3	109.2(3)
Ag11–Au3–P3	123.9(7)	Au4–AP11–Au13	113.7(2)	Ag4–Au13–Ag4	60.3(3)	Ag1–Ag2–Cl2	112.4(9)
Ag2–Au3–Ag3	61.3(2)	Au4–AP11–Ag11	65.4(2)	Ag4–Au13–Ag5	60.5(2)	Ag2–Ag2–Ag3	88.3(3)
Ag2–Au3–P3	121.0(7)	Au4–AP11–Ag1	175.0(2)	Ag4–Au13–Ag5	91.1(2)	Ag2–Ag2–Cl2	52.1(5)
Ag3–Au3–P3	114.1(7)	Au4–AP11–Ag2	118.8(2)	Ag5–Au13–Ag5	61.2(2)	Ag3–Ag2–Cl2	120.1(9)
Au3–Au4–Au5	108.9(1)	Au4–AP11–Ag3	64.7(2)	Au1–Ag11–Au2	58.0(2)	Au3–Ag3–Au4	59.8(2)
Au3–Au4–AP11	57.4(1)	Au4–AP11–Ag4	61.9(2)	Au1–Ag11–Au3	102.1(2)	Au3–Ag3–AP11	56.7(2)
Au3–Au4–Ag11	62.5(2)	Au4–AP11–Ag5	114.6(2)	Au1–Ag11–Au4	103.1(2)	Au3–Ag3–Au13	108.4(2)
Au3–Au4–Ag3	57.6(2)	Au5–AP11–Au13	113.5(2)	Au1–Ag11–Au5	57.9(2)	Au3–Ag3–Ag2	61.0(2)
Au3–Au4–Ag4	107.7(2)	Au5–AP11–Ag11	65.3(2)	Au1–Ag11–AP11	54.9(2)	Au3–Ag3–Ag3	151.0(3)
Au3–Au4–P4	122.8(5)	Au5–AP11–Ag1	115.3(2)	Au1–Ag11–Cl11	123.6(8)	Au3–Ag3–Ag4	106.8(3)
Au5–Au4–AP11	58.1(1)	Au5–AP11–Ag2	174.5(2)	Au2–Ag11–Au3	58.0(2)	Au3–Ag3–Cl3	124.8(6)
Au5–Au4–Ag11	60.8(2)	Au5–AP11–Ag3	118.4(2)	Au2–Ag11–Au4	104.1(2)	Au4–Ag3–AP11	55.3(2)
Au5–Au4–Ag3	109.0(2)	Au5–AP11–Ag4	63.6(2)	Au2–Ag11–Au5	104.7(3)	Au4–Ag3–Au13	105.1(2)
Au5–Au4–Ag4	61.2(2)	Au5–AP11–Ag5	61.7(2)	Au2–Ag11–AP11	56.3(2)	Au4–Ag3–Ag2	107.1(3)
Au5–Au4–P4	121.4(5)	Au13–AP11–Ag11	178.6(2)	Au2–Ag11–Cl11	123.9(8)	Au4–Ag3–Ag3	145.7(3)
AP11–Au4–Ag11	58.8(1)	Au13–AP11–Ag1	61.4(2)	Au3–Ag11–Au4	57.6(2)	Au4–Ag3–Ag4	57.5(2)
AP11–Au4–Ag3	60.0(2)	Au13–AP11–Ag2	61.8(2)	Au3–Ag11–Au5	103.7(2)	Au4–Ag3–Cl3	134.3(7)
AP11–Au4–Ag4	61.3(2)	Au13–AP11–Ag3	60.8(2)	Au3–Ag11–AP11	54.8(2)	AP11–Ag3–Au13	59.6(1)

Table 4 (Continued)

(a) $[(Ph_3P)_{10}Au_{12}Ag_{12}PtCl_7]Cl$ (**1**)

AP11–Ag3–Ag2	58.3(2)	AP11–Ag4–Au13	59.7(2)	Au5–Ag5–Cl5	123.7(8)	Au2–P2–C2A1	114(1)
AP11–Ag3–Ag3	119.2(3)	AP11–Ag4–Ag3	59.0(2)	AP11–Ag5–Au13	59.7(1)	Au2–P2–C2B1	112(1)
AP11–Ag3–Ag4	58.4(2)	AP11–Ag4–Ag4	119.5(3)	AP11–Ag5–Ag1	58.9(2)	Au2–P2–C2C1	117(1)
AP11–Ag3–Cl3	170.4(8)	AP11–Ag4–Ag5	58.9(2)	AP11–Ag5–Ag4	59.0(2)	C2A1–P2–C2B1	110(1)
Au13–Ag3–Ag2	60.0(2)	AP11–Ag4-Cl4	171.0(7)	AP11–Ag5–Ag5	119.1(3)	C2A1–P2–C2C1	100(1)
Ag13–Ag3–Ag3	59.6(2)	Au13–Ag4–Ag3	59.1(2)	AP11–Ag5–Cl5	170.5(8)	C2B1–P2–C2C1	103(1)
Au13–Ag3–Ag4	59.4(2)	Au13–Ag4–Ag4	59.9(2)	Au13–Ag5–Ag1	59.6(2)	Au3–P3–C3A1	114(1)
Au13–Ag3–Cl3	113.2(5)	Au13–Ag4–Ag5	59.8(2)	Au13–Ag5–Ag4	59.7(2)	Au3–P3–C3B1	117(1)
Ag2–Ag3–Ag3	91.7(3)	Au13–Ag4–Cl4	114.0(6)	Au13–Ag5-Ag5	59.4(2)	Au3–P3–C3C1	114(1)
Ag2–Ag3–Ag4	107.2(2)	Ag3–Ag4–Ag4	90.1(3)	Au13–Ag5–Cl5	113.1(5)	C3A1–P3–C3B1	107(1)
Ag2–Ag3–Cl3	113.2(8)	Ag3–Ag4–Ag5	107.7(3)	Ag1–Ag5–Ag4	107.9(2)	C3A1–P3–C3C1	105(1)
Ag3–Ag3–Ag4	89.9(3)	Ag3–Ag4–Cl4	112.6(7)	Ag1–Ag5–Ag5	90.7(3)	C3B1–P3–C3C1	98(1)
Ag3–Ag3–Cl3	54.2(4)	Ag4–Ag4–Ag5	90.4(3)	Ag1–Ag5–Cl5	124.5(9)	Au4–P4–C4A1	114(1)
Ag4–Ag3–Cl3	125.0(8)	Ag4–Ag4–Cl4	54.6(5)	Ag4–Ag5–Ag5	89.6(3)	Au4–P4–C4B1	115(1)
Au4–Ag4–Au5	60.8(2)	Ag5–Ag4–Cl4	125.0(8)	Ag4–Ag5–Cl5	112.5(9)	Au4–P4–C4C1	112(1)
Au4–Ag4–AP11	56.8(2)	Au1–Ag5–Au5	61.2(2)	Ag5–Ag5–Cl5	54.1(5)	C4A1–P4–C4B1	109(1)
Au4–Ag4–Au13	108.1(2)	Au1–Ag5–AP11	56.4(2)	Ag1–Cl1–Ag1	72(1)	C4A1–P4–C4C1	93(1)
Au4–Ag4–Ag3	61.6(2)	Au1–Ag5–Au13	106.3(2)	Ag2–Cl2–Ag2	76(1)	C4B1–P4–C4C1	111(1)
Au4–Ag4–Ag4	149.7(2)	Au1–Ag5–Ag1	58.5(2)	Ag3–Cl3–Ag3	71.7(8)	Au5–P5–C5A1	110(1)
Au4–Ag4–Ag5	107.7(3)	Au1–Ag5–Ag4	108.8(2)	Ag4–Cl4-Ag4	71(1)	Au5–P5–C5B1	113(1)
Au4–Ag4–Cl4	123.8(7)	Au1–Ag5–Ag5	147.4(3)	Ag5–Cl5–Ag5	72(1)	Au5–P5–C5C1	111(1)
Au5–Ag4–AP11	56.7(2)	Au1–Ag5–Cl5	133.1(7)	Au1–P1–C1A1	114(1)	C5A1–P5–C5B1	104(1)
Au5–Ag4–Au13	106.6(2)	Au5–Ag5–AP11	57.7(2)	Au1–P1–C1B1	112(1)	C5A1–P5–C5C1	117(2)
Au5–Ag4–Ag3	109.3(3)	Au5–Ag5–Au13	108.7(2)	Au1–P1–C1C1	114(1)	C5B1–P5–C5C1	102(1)
Au5–Ag4–Ag4	146.7(3)	Au5–Ag5–Ag1	108.6(3)	C1A1–P1–C1B1	97(1)		
Au5–Ag4–Ag5	58.4(2)	Au5–Ag5–Ag4	61.2(2)	C1A1–P1–C1C1	107(1)		
Au5–Ag4–Cl4	132.2(6)	Au5–Ag5–Ag5	148.5(3)	C1B1–P1–C1C1	110(2)		

(b) $[(Ph_3P)_{10}Au_{12}Ag_{12}NiCl_7]SbF_6$ (**4**)

Au2–Au1–Au5	107.6(2)	Au4–Au3–Ag2	108.7(3)	Ag11–Au5–Ag5	111.1(4)	Au13–Au11–Ag11	179.5(4)
Au2–Au1–Au11	58.0(2)	Au4–Au3–Ag3	61.9(3)	Ag11–Au5–P5	124(1)	Au13–Au11–Ag1	60.9(4)
Au2–Au1–Ag11	59.5(3)	Au4–Au3–P3	119(1)	Ag4–Au5–Ag5	60.1(3)	Au13–Au11–Ag2	61.5(3)
Au2–Au1–Ag1	62.7(3)	Au11–Au3–Ag11	57.7(2)	Ag4–Au5–P5	119(1)	Au13–Au11–Ag3	61.2(4)
Au2–Au1–Ag5	111.1(3)	Au11–Au3–Ag2	59.9(3)	Ag5–Au5–P5	117(1)	Au13–Au11–Ag4	61.9(4)
Au2–Au1–P1	121(1)	Au11–Au3–Ag3	61.7(3)	Au1–Au11–Au2	64.9(2)	Au13–Au11–Ag5	61.8(3)
Au5–Au1–Au11	58.0(2)	Au11–Au3–P3	175(1)	Au1–Au11–Au3	122.6(4)	Ag11–Au11–Ag1	119.2(5)
Au5–Au1–Ag11	60.2(3)	Ag11–Au3–Ag2	108.2(3)	Au1–Au11–Au4	121.5(3)	Ag11–Au11–Ag2	119.0(4)
Au5–Au1–Ag1	109.6(3)	Ag11–Au3–Ag3	111.4(3)	Au1–Au11–Au5	65.3(2)	Ag11–Au11–Ag3	119.0(4)
Au5–Au1–Ag5	58.7(3)	Ag11–Au3–P3	124.3(9)	Au1–Au11–Au13	112.7(4)	Ag11–Au11–Ag4	117.8(5)
Au5–Au1–P1	125(1)	Ag2–Au3–Ag3	61.1(4)	Au1–Au11–Ag11	67.1(3)	Ag11–Au11–Ag5	117.7(4)
Au11–Au1–Ag11	58.1(3)	Ag2–Au3–P3	121.0(9)	Au1–Au11–Ag1	62.0(3)	Ag1–Au11–Ag2	60.8(3)
Au11–Au1–Ag1	61.5(3)	Ag3–Au3–P3	114(1)	Au1–Au11–Ag2	114.0(4)	Ag1–Au11–Ag3	112.1(4)
Au11–Au1–Ag5	60.8(3)	Au3–Au4–Au5	109.2(2)	Au1–Au11–Ag3	173.7(4)	Ag1–Au11–Ag4	113.4(4)
Au11–Au1–P1	176(1)	Au3–Au4–Au11	57.8(2)	Au1–Au11–Ag4	116.7(3)	Ag1–Au11–Ag5	63.4(3)
Ag11–Au1–Ag1	111.3(3)	Au3–Au4–Ag11	62.3(3)	Au1–Au11–Ag5	62.8(3)	Ag2–Au11–Ag3	62.3(3)
Ag11–Au1–Ag5	108.9(3)	Au3–Au4–Ag3	57.9(3)	Au2–Au11–Au3	65.2(2)	Ag2–Au11–Ag4	114.1(4)
Ag11–Au1–P1	125(1)	Au3–Au4–Ag4	107.9(3)	Au2–Au11–Au4	119.4(3)	Ag2–Au11–Ag5	113.7(4)
Ag1–Au1–Ag5	62.6(3)	Au3–Au4–P4	123.7(8)	Au2–Au11–Au5	119.2(3)	Ag3–Au11–Ag4	62.8(3)
Ag1–Au1–P1	115(1)	Au5–Au4–Au11	58.2(2)	Au2–Au11–Au13	115.7(4)	Ag3–Au11–Ag5	113.2(4)
Ag5–Au1–P1	118(1)	Au5–Au4–Ag11	60.9(2)	Au2–Au11–Ag11	64.6(3)	Ag4–Au11–Ag5	61.5(3)
Au1–Au2–Au3	108.8(2)	Au5–Au4–Ag3	109.3(3)	Au2–Au11–Ag1	65.2(3)	Au11–Au13–Au11	177.5(5)
Au1–Au2–Au11	57.1(2)	Au5–Au4–Ag4	60.8(3)	Au2–Au11–Ag2	63.3(3)	Au11–Au13–Ag1	59.6(3)
Au1–Au2–Ag11	62.5(2)	Au5–Au4–P4	121.9(8)	Au2–Au11–Ag3	115.4(3)	Au11–Au13–Ag1	122.3(4)
Au1–Au2–Ag1	57.8(3)	Au11–Au4–Ag11	58.6(3)	Au2–Au11–Ag4	177.4(4)	Au11–Au13–Ag2	59.0(3)
Au1–Au2–Ag2	105.4(3)	Au11–Au4–Ag3	60.3(3)	Au2–Au11–Ag5	118.6(4)	Au11–Au13–Ag2	123.1(4)
Au1–Au2–P2	123.0(8)	Au11–Au4–Ag4	60.9(3)	Au3–Au11–Au4	64.9(3)	Au11–Au13–Ag3	59.6(3)
Au3–Au2–Au11	57.3(2)	Au11–Au4–P4	177(1)	Au3–Au11–Au5	120.9(4)	Au11–Au13–Ag3	119.8(4)
Au3–Au2–Ag11	62.5(3)	Ag11–Au4–Ag3	109.8(4)	Au3–Au11–Au13	113.3(3)	Au11–Au13–Ag4	58.5(3)
Au3–Au2–Ag1	106.2(3)	Ag11–Au4–Ag4	110.9(3)	Au3–Au11–Ag11	67.2(4)	Au11–Au13–Ag4	119.0(4)
Au3–Au2–Ag2	60.1(3)	Ag11–Au4–P4	124(1)	Au3–Au11–Ag1	117.2(4)	Au11–Au13–Ag5	58.9(3)
Au3–Au2–P2	119.7(8)	Ag3–Au4–Ag4	61.2(4)	Au3–Au11–Ag2	63.8(3)	Au11–Au13–Ag5	120.2(3)
Au11–Au2–Ag11	59.0(3)	Ag3–Au4–P4	117.8(9)	Au3–Au11–Ag3	61.3(3)	Au11–Au13–Ag1	122.3(4)
Au11–Au2–Ag1	59.3(3)	Ag4–Au4–P4	116.3(9)	Au3–Au11–Ag4	114.4(4)	Au11–Au13–Ag1	59.6(3)
Au11–Au2–Ag2	60.0(3)	Au1–Au5–Au4	107.5(2)	Au3–Au11–Ag5	174.5(4)	Au11–Au13–Ag2	123.1(4)
Au11–Au2–P2	175(1)	Au1–Au5–Au11	56.7(2)	Au4–Au11–Au5	64.7(2)	Au11–Au13–Ag2	59.0(3)
Ag11–Au2–Ag1	109.7(3)	Au1–Au5–Ag11	61.7(3)	Au4–Au11–Au13	114.1(4)	Au11–Au13–Ag3	119.8(4)
Ag11–Au2–Ag2	111.4(4)	Au1–Au5–Ag4	106.7(3)	Au4–Au11–Ag11	65.9(4)	Au11–Au13–Ag3	59.6(3)
Ag11–Au2–P2	116(1)	Au1–Au5–Ag5	59.8(3)	Au4–Au11–Ag1	174.9(5)	Au11–Au13–Ag4	119.0(4)
Ag1–Au2–Ag2	58.0(3)	Au1–Au5–P5	123(1)	Au4–Au11–Ag2	118.3(3)	Au11–Au13–Ag4	58.5(3)
Ag1–Au2–P2	125.9(9)	Au4–Au5–Au11	57.1(2)	Au4–Au11–Ag3	64.3(3)	Au11–Au13–Ag5	120.2(3)
Ag2–Au2–P2	123.4(9)	Au4–Au5–Ag11	60.9(3)	Au4–Au11–Ag4	61.9(3)	Au11–Au13–Ag5	58.9(3)
Au2–Au3–Au4	106.7(2)	Au4–Au5–Ag4	58.3(3)	Au4–Au11–Ag5	114.1(4)	Ag1–Au13–Ag1	62.7(4)
Au2–Au3–Au11	57.5(2)	Au4–Au5–Ag5	107.3(3)	Au5–Au11–Au13	114.1(3)	Ag1–Au13–Ag2	59.6(3)
Au2–Au3–Ag11	59.1(2)	Au4–Au5–P5	125(1)	Au5–Au11–Ag11	65.4(3)	Ag1–Au13–Ag2	92.6(4)
Au2–Au3–Ag2	59.6(3)	Au11–Au5–Ag11	58.3(3)	Au5–Au11–Ag1	115.8(3)	Ag1–Au13–Ag3	109.7(4)
Au2–Au3–Ag3	109.5(3)	Au11–Au5–Ag4	59.6(3)	Au5–Au11–Ag2	175.2(4)	Ag1–Au13–Ag3	149.2(4)
Au2–Au3–P3	127(1)	Au11–Au5–Ag5	60.8(3)	Au5–Au11–Ag3	117.9(4)	Ag1–Au13–Ag4	109.6(4)
Au4–Au3–Au11	57.3(2)	Au11–Au5–P5	177(1)	Au5–Au11–Ag4	63.3(3)	Ag1–Au13–Ag4	149.2(4)
Au4–Au3–Ag11	60.2(3)	Ag11–Au5–Ag4	108.9(3)	Au5–Au11–Ag5	61.5(3)	Ag1–Au13–Ag5	61.9(3)

Table IV (Continued)

(b) $[(Ph_3P)_{10}Au_{12}Ag_{12}NiCl_7]SbF_6$ (4)

Ag1–Au13–Ag5	93.5(4)	Au13–Ag1–Ag1	58.7(3)	Au13–Ag3–Ag2	59.5(3)	Au13–Ag5–Ag1	58.5(4)
Ag2–Au13–Ag2	64.1(4)	Au13–Ag1–Ag2	60.5(3)	Au13–Ag3–Ag3	59.9(3)	Au13–Ag5–Ag4	60.2(3)
Ag2–Au13–Ag3	60.9(3)	Au13–Ag1–Ag5	59.6(3)	Au13–Ag3–Ag4	59.6(3)	Au13–Ag5–Ag5	59.3(3)
Ag2–Au13–Ag3	92.6(4)	Au13–Ag1–Cl1	112.8(9)	Au13–Ag3–Cl3	113(1)	Au13–Ag5–Cl5	113(1)
Ag2–Au13–Ag4	109.2(3)	Ag1–Ag1–Ag2	90.8(4)	Ag2–Ag3–Ag3	91.6(5)	Ag1–Ag5–Ag4	107.4(4)
Ag2–Au13–Ag4	149.7(4)	Ag1–Ag1–Ag5	89.8(5)	Ag2–Ag3–Ag4	106.9(4)	Ag1–Ag5–Ag5	90.2(4)
Ag2–Au13–Ag5	109.2(3)	Ag1–Ag1–Cl1	54.6(8)	Ag2–Ag3–Cl3	109(2)	Ag1–Ag5–Cl5	126(2)
Ag2–Au13–Ag5	150.4(5)	Ag2–Ag1–Ag5	108.0(5)	Ag3–Ag3–Ag4	90.2(4)	Ag4–Ag5–Ag5	89.6(4)
Ag3–Au13–Ag3	60.2(4)	Ag2–Ag1–Cl1	113(1)	Ag3–Ag3–Cl3	54.7(8)	Ag4–Ag5–Cl5	111(2)
Ag3–Au13–Ag4	61.1(3)	Ag5–Ag1–Cl1	124(1)	Ag4–Ag3–Cl3	130(1)	Ag5–Ag5–Cl5	54.3(8)
Ag3–Au13–Ag4	91.2(4)	Au2–Ag2–Au3	60.3(3)	Au4–Ag4–Au5	60.9(3)	Ag1–Cl1–Ag1	71(2)
Ag3–Au13–Ag5	109.4(3)	Au2–Ag2–Au11	56.7(3)	Au4–Ag4–Au11	57.2(3)	Ag2–Cl2–Ag2	75(1)
Ag3–Au13–Ag5	147.6(5)	Au2–Ag2–Au13	108.5(3)	Au4–Ag4–Au13	108.2(3)	Ag3–Cl3–Ag3	71(2)
Ag4–Au13–Ag4	60.5(4)	Au2–Ag2–Ag1	62.5(3)	Au4–Ag4–Ag3	61.5(3)	Ag4–Cl4–Ag4	70(2)
Ag4–Au13–Ag5	59.4(3)	Au2–Ag2–Ag2	150.6(4)	Au4–Ag4–Ag4	149.2(4)	Ag5–Cl5–Ag5	71(2)
Ag4–Au13–Ag5	90.3(4)	Au2–Ag2–Ag3	107.4(4)	Au4–Ag4–Ag5	108.4(5)	Au1–P1–C1A1	125(2)
Ag5–Au13–Ag5	61.3(3)	Au2–Ag2–Cl2	126.9(9)	Au4–Ag4–Cl4	120(1)	Au1–P1–C1B1	115(2)
Au1–Ag11–Au2	58.0(3)	Au3–Ag2–Au11	56.4(3)	Au5–Ag4–Au11	57.1(3)	Au1–P1–C1C1	116(2)
Au1–Ag11–Au3	102.4(4)	Au3–Ag2–Au13	105.7(4)	Au5–Ag4–Au13	107.1(4)	C1A1–P1–C1B1	105(2)
Au1–Ag11–Au4	102.7(4)	Au3–Ag2–Ag1	109.9(4)	Au5–Ag4–Ag3	109.6(4)	C1A1–P1–C1C1	90(2)
Au1–Ag11–Au5	58.1(2)	Au3–Ag2–Ag2	144.9(5)	Au5–Ag4–Ag4	147.2(4)	C1B1–P1–C1C1	101(2)
Au1–Ag11–Au11	54.8(3)	Au3–Ag2–Ag3	58.0(3)	Au5–Ag4–Ag5	58.8(3)	Au2–P2–C2A1	114(2)
Au1–Ag11–Cl11	124(1)	Au3–Ag2–Cl2	136.1(8)	Au5–Ag4–Cl4	135(1)	Au2–P2–C2B1	110(2)
Au2–Ag11–Au3	58.4(2)	Au11–Ag2–Au13	59.6(3)	Au11–Ag4–Au13	59.6(3)	Au2–P2–C2C1	112(2)
Au2–Ag11–Au4	104.0(4)	Au11–Ag2–Ag1	59.9(3)	Au11–Ag4–Ag3	59.3(3)	C2A1–P2–C2B1	102(2)
Au2–Ag11–Au5	104.7(4)	Au11–Ag2–Ag2	117.5(4)	Au11–Ag4–Ag4	119.3(5)	C2A1–P2–C2C1	108(2)
Au2–Ag11–Au11	56.4(3)	Au11–Ag2–Ag3	59.3(4)	Au11–Ag4–Ag5	59.5(4)	C2B1–P2–C2C1	110(2)
Au2–Ag11–Cl11	126(1)	Au11–Ag2–Cl2	167.5(8)	Au11–Ag4–Cl4	167(1)	Au3–P3–C3A1	104(2)
Au3–Ag11–Au4	57.5(2)	Au13–Ag2–Ag1	59.9(3)	Au13–Ag4–Ag3	59.3(3)	Au3–P3–C3B1	112(2)
Au3–Ag11–Au5	103.3(4)	Au13–Ag2–Ag2	58.0(3)	Au13–Ag4–Ag4	59.8(3)	Au3–P3–C3C1	115(2)
Au3–Ag11–Au11	55.1(3)	Au13–Ag2–Ag3	59.7(3)	Au13–Ag4–Ag5	60.4(3)	C3A1–P3–C3B1	118(2)
Au3–Ag11–Cl11	127.1(9)	Au13–Ag2–Cl2	109.9(7)	Au13–Ag4–Cl4	114(1)	C3A1–P3–C3C1	105(1)
Au4–Ag11–Au5	58.2(3)	Ag1–Ag2–Ag2	89.2(4)	Ag3–Ag4–Ag4	89.8(4)	C3B1–P3–C3C1	104(2)
Au4–Ag11–Au11	55.5(3)	Ag1–Ag2–Ag3	108.9(4)	Ag3–Ag4–Ag5	108.7(4)	Au4–P4–C4A1	116(2)
Au4–Ag11–Cl11	124(1)	Ag1–Ag2–Cl2	110(1)	Ag3–Ag4–Cl4	108(1)	Au4–P4–C4B1	112(2)
Au5–Ag11–Au11	56.2(3)	Ag2–Ag2–Ag3	88.4(4)	Ag4–Ag4–Ag5	90.4(5)	Au4–P4–C4C1	113(1)
Au5–Ag11–Cl11	121(1)	Ag2–Ag2–Cl2	52.6(6)	Ag4–Ag4–Cl4	55.1(9)	C4A1–P4–C4B1	110(2)
Au11–Ag11–Cl11	177(1)	Ag3–Ag2–Cl2	123(1)	Ag5–Ag4–Cl4	129(1)	C4A1–P4–C4C1	103(2)
Au1–Ag1–Au2	59.5(3)	Au3–Ag3–Au4	60.2(3)	Au1–Ag5–Au5	61.6(3)	C4B1–P4–C4C1	100(2)
Au1–Ag1–Au11	56.5(3)	Au3–Ag3–Au11	57.0(3)	Au1–Ag5–Au11	56.4(3)	Au5–P5–C5A1	120(2)
Au1–Ag1–Au13	107.0(4)	Au3–Ag3–Au13	107.9(4)	Au1–Ag5–Au13	105.4(3)	Au5–P5–C5B1	110(2)
Au1–Ag1–Ag1	147.1(4)	Au3–Ag3–Ag2	60.9(3)	Au1–Ag5–Ag1	58.3(3)	Au5–P5–C5C1	116(2)
Au1–Ag1–Ag2	108.0(5)	Au3–Ag3–Ag3	150.7(5)	Au1–Ag5–Ag4	108.8(5)	C5A1–P5–C5B1	103(2)
Au1–Ag1–Ag5	59.1(3)	Au3–Ag3–Ag4	106.7(4)	Au1–Ag5–Ag5	146.7(5)	C5A1–P5–C5C1	101(2)
Au1–Ag1–Cl1	133(1)	Au3–Ag3–Cl3	121(1)	Au1–Ag5–Cl5	135(2)	C5B1–P5–C5C1	104(2)
Au2–Ag1–Au11	55.5(3)	Au4–Ag3–Au11	55.4(3)	Au5–Ag5–Au11	57.7(3)	F1–Sb–F2	83.5(6)
Au2–Ag1–Au13	106.6(4)	Au4–Ag3–Au13	105.1(3)	Au5–Ag5–Au13	108.7(3)	F1–Sb–F3	87.7(7)
Au2–Ag1–Ag1	149.2(4)	Au4–Ag3–Ag2	107.2(4)	Au5–Ag5–Ag1	108.4(4)	F1–Sb–F4	97.8(5)
Au2–Ag1–Ag2	59.5(3)	Au4–Ag3–Ag3	145.7(4)	Au5–Ag5–Ag4	61.1(4)	F1–Sb–F5	93.0(6)
Au2–Ag1–Ag5	106.0(5)	Au4–Ag3–Ag4	57.4(3)	Au5–Ag5–Ag5	148.5(5)	F2–Sb–F3	113(1)
Au2–Ag1–Cl1	127(1)	Au4–Ag3–Cl3	137(1)	Au5–Ag5–Cl5	123(1)	F2–Sb–F4	161(1)
Au11–Ag1–Au13	59.5(3)	Au11–Ag3–Au13	59.2(3)	Au11–Ag5–Au13	59.3(2)	F2–Sb–F5	72.8(8)
Au11–Ag1–Ag1	118.2(5)	Au11–Ag3–Ag2	58.4(3)	Au11–Ag5–Ag1	58.6(3)	F3–Sb–F4	86.4(8)
Au11–Ag1–Ag2	59.3(3)	Au11–Ag3–Ag3	119.1(4)	Au11–Ag5–Ag4	58.9(3)	F3–Sb–F5	175(1)
Au11–Ag1–Ag5	58.0(3)	Au11–Ag3–Ag4	57.9(3)	Au11–Ag5–Ag5	118.6(4)	F4–Sb–F5	88(1)
Au11–Ag1–Cl1	171(1)	Au11–Ag3–Cl3	167(2)	Au11–Ag5–Cl5	169(2)		

in *metal–metal* and *metal–ligand* interactions, as well as in the electronegativity of the constituents. In terms of metal–metal interactions, which is related to the cohesive energy (368 for Au vs 285 for Ag, in kJ/mol), gold atoms tend to prefer interstitial sites such as the centers of icosahedra (rule 1) or the shared vertices (rule 2). As far as the metal–ligand bonding is concerned, the more electron-donating phosphine ligands prefer to coordinate to the more electronegative Au atoms (rule 3), whereas the more electron-withdrawing halide ligands prefer to interact with the more electropositive Ag atoms (rule 6). In terms of electronegativity, which is related to relativistic effects,[21,22] the more electronegative gold atoms (2.54 for Au vs 1.93 for Ag) prefer sites of high electron densities (such as the centers of icosahedra or the shared vertices) whereas the more electropositive silver atoms tend to occupy either surface sites (at the boundary of adjacent icosahedra) bridged by halide ligands (rule 4) or capping positions with high halide coordination (rule 5).

(2) Trimetallic Au–Ag–M (M = Group 10 Metals) Supraclusters. For mixed group 10 (M)–group 11 clusters such as the trimetallic Au–Ag–M supraclusters considered here, the site preference (summarized in Chart 2) can be attributed to the relative strengths of *metal–metal* and *metal–ligand* interactions as well as disparities in electronegativity: (1) group 10 metals prefer interstitial sites such as the centroids of icosahedra due to their high cohesive energies (M > Au > Ag) that lead to stronger metal–metal bonds;[20] (2) among the group 11 metals, Au prefers the interstitial sites such as the centers of icosahedra or the shared

(21) (a) Pyykko, P.; Desclaux, J. *Acc. Chem. Res.* **1979**, *12*, 276. (b) Pitzer, K. S. *ibid.* **1979**, *12*, 271.

(22) (a) Grohmann, A.; Riede, J.; Schmidbaur, H. *Nature* **1990**, *345*, 140. (b) Scherbaum, F.; Grohmann, A.; Muller, G.; Schmidbaur, H. *Angew. Chem., Int. Ed. Engl.* **1989**, *28*, 463. (c) Schmidbaur, H.; Graf, W.; Muller, G. *Angew. Chem., Int. Ed. Engl.* **1988**, *27*, 417. (d) Schmidbaur, H.; Scherbaum, F.; Huber, B.; Muller, G. *Angew. Chem., Int. Ed. Engl.* **1988**, *27*, 419.

Chart 2

	Site Preference
Center	Ni, Pd, Pt > Au
Vertex	Au > Ag
Surface P	Au > Ag
Surface X	Au < Ag

Chart 3

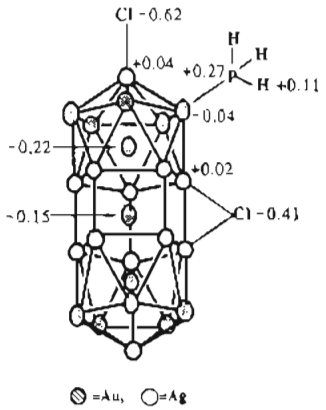

vertices due to its high cohesive energy and high electronegativity (Au > Ag); and (3) as far as the metal–ligand bonding is concerned, the more electronegative Au prefers phosphine coordination while the more electropositive Ag prefers halide coordination or halide bridging.

(3) Molecular Orbital Calculations: Preliminary Results. To further assess the electronic origins of the site preference, we have performed extended Huckel molecular orbital (EHMO) calculations[23] on the bimetallic cluster $[(R_3P)_{10}Au_{13}Ag_{12}Cl_7]^{2+}$ where R = H. Preliminary results show that the *overall* metal–metal-bonding strength follows the trend[24] of centers of icosahedra > shared vertices > surface sites. In other words, the strong preference for the group 10 (e.g., Ni) metal to occupy the center position stems from the fact that the sum (12 each) of the overlap populations (op) of the metal–metal bonds emanating from the center is substantially larger than that emanating from the shared vertex; in turn, both of these values are significantly greater than the corresponding values calculated for the various surface sites (excluding metal–ligand bonds). The same argument applies to Au vs Ag within the group 11 metals with Au preferring the interstitial sites. In terms of metal–ligand bonding, the average overlap population per bond follows the trend of Au–P > terminal Ag–Cl > bridging Ag–Cl. In terms of electronegativity, the observed site preference is in accord with the calculated charge distribution depicted in Chart 3. Here, metal atoms of relatively high electronegativity (Au > Ag) prefer sites of high electron density (which follow the trend of centers of icosahedra > shared vertices > phosphine-coordinated > halide-coordinated).

The average overlap populations per metal–metal (M–M) bond calculated for the different pairs of the metal sites follow these trends: (1) (radial) M_c–M_v > M_s–M_s (tangential) within each icosahedron and (2) intraicosahedral ≫ intericosahedral. Here the subscripts c, v, and s denote centers of icosahedra, the shared vertex, and "surface" metal atoms, respectively. These trends correlate nicely with the relative orderings of the observed intermetallic distances: (1) M–Au < M–Ag < Au–Au ≤ Au–Ag <Ag–Ag (M = group 10 metals); (2) M_c–M_s < M_c–M_v < M_v–M_s < M_s–M_s; (3) intraicosahedral < intericosahedral.

(IV) Site Preference in Metal Alloy Systems: Generalizations

(A) Metal–Metal Interactions: Bond Strength vs Charge Accumulation (BSCA) Plots. The general principles developed in the previous section can be extended to other mixed-metal clusters. In fact, if we focus our attention on the *metal–metal interactions only*, the site preference of any metal alloy systems can be inferred from a plot of bond strengths vs charge (electron densities) accumulation of the constituents as exemplified by Figure 3a–c for a bi-, a tri-, and a tetrametallic alloy system, respectively. In Figure 3, the metal–metal bond strength is represented by the bond energy, estimated from the cohesive energy, whereas the ability of the constituent metals to accumulate negative charges (i.e., electron densities) is based on Pauling's electronegativity. We shall refer to these figures as bond strength vs charge accumulation (BSCA) plots. The bond energy per metal–metal bond (E_b) in bulk metal can be calculated from the heat of formation, $\Delta H°_f$, as follows:

$$E_b = 2\Delta H°_f/N \qquad (1)$$

Here, N is the coordination number. For face-centered cubic metals, $N = 12$. We shall take this as a measure of the relative bond strength for a homonuclear metal–metal bond. For a heteronuclear metal–metal bond, we shall use the arithmatic mean of the bond energies of the constituents:

$$E_{b12} = (E_{b1} + E_{b2})/2 \qquad (2)$$

In Figure 3, the locations of the metal constituents indicate their homonuclear bond strengths (ordinate) and charge accumulation (abscissa) capabilities whereas the lines connecting them designate variations of these two properties for the heteronuclear bonds. (For a mixed-metal system containing n different types of metals, we should have a n-sided polygon with $C^n_2 = n(n-1)/2$ lines connecting the n vertices.) The bond energies for homonuclear metal–metal bonds (calculated on the basis of eq 1) can be read from the ordinate; the corresponding bond energies for heteronuclear metal–metal bonds (calculated via eq 2) can be determined from the ordinate of the midpoints of the lines connecting the two metals.

The site preference for a metal alloy system can now be predicted from the BSCA plot. Before we do that, however, we must first discuss the differences between interstitial vs surface sites and their bonding consequences. If we ignore metal–ligand bonding (which will be discussed later) and focus our attention on metal–metal bonding only, there are two characteristics that distinguish interstitial sites from surface sites. First is the large number of nearest neighbors and hence the large number of metal–metal bonds. In the case of an icosahedral cluster, the 12 radial bonds emanating from the interstitial atom are also among the shortest in the cluster. The combination of numerous and stronger bonds associated with the interstitial atom in a cluster[20] implies that metals with stronger bond strengths tend to occupy the interstitial sites due to the greater gain in stabilization energy, both in number and in magnitude. The second characteristic is the accumulation of electron densities at the center of a cluster. As a result, the more electronegative metal atoms tend to occupy the interstitial sites whereas metals at the lower left corner tend to be on the surface of the cluster. For example, for the Au–Ag system, the BSCA plot (Figure 3a) predicts that Au should occupy the interstitial sites such as the centers of the icosahedra.

The wide ranges of bond strength and electronegativity of transition metals imply that both factors are important in determining the site preference in mixed-metal clusters. In fact, four cases can be distinguished. The first case involves metals with similar electronegativities but different bonding strengths

(23) Teo, B. K.; Zhang, H. To be published.
(24) Similar trends were obtained from calculations performed on the pure gold analog $[(R_3P)_{10}Au_{25}Cl_7]^{2+}$ dication (R = H).

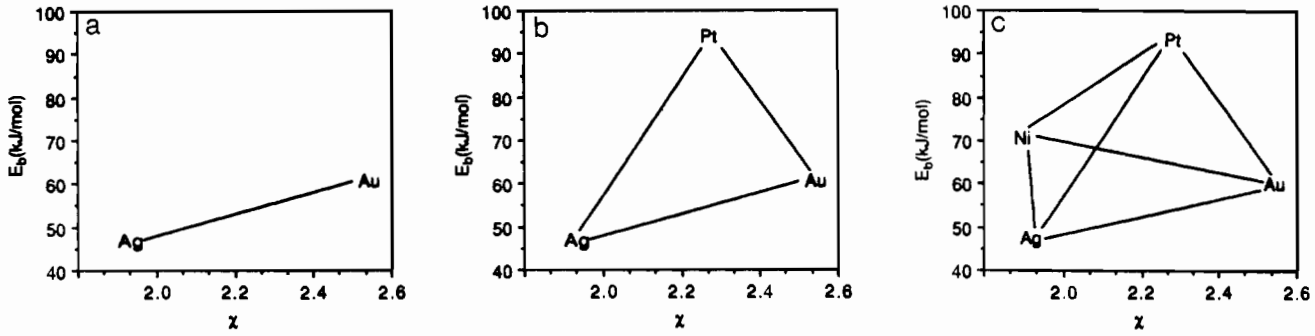

Figure 3. Bond strengths vs charge (electron density) accumulation (BSCA) plots for (a) bimetallic Au–Ag, (b) trimetallic Au–Ag–Pt, and (c) tetrametallic Au–Ag–Pt–Ni systems. Here the metal–metal bond strength is represented by the bond energy (E_b), estimated from the cohesive energy whereas the ability of the constitutent metals to accumulate negative charge (i.e., electron densities) is estimated by using Pauling's electronegativity (χ). The bond energies for homonuclear metal–metal bonds (calculated on the basis of eq 1) can be read from the ordinate while the corresponding bond energies for heteronuclear metal–metal bonds (calculated via eq 2) can be determined from the ordinate of the midpoints of the lines connecting the two metals.

	Average M-M distance(Å)	M-M bond energy (kJ/mol)
Pt-Pt	--	94.3
Pt-Au	2.69	77.8
Pt-Ag	2.81	70.9
Au-Au	2.88	61.4
Au-Ag	2.88	54.4
Ag-Ag	2.90 2.95	47.5

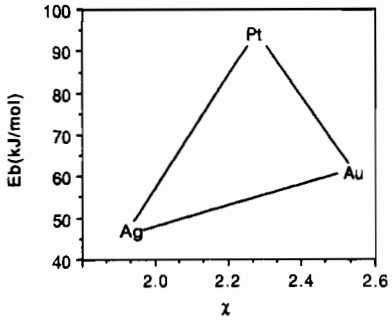

Figure 4. BSCA plot of a trimetallic Au–Ag–Pt system (same as Figure 3b). As shown in the left margin, the five observed average metal–metal distances (in Å) in **1** follow a trend which is opposite to the corresponding trend of the bond energies (E_b) (in kJ/mol).

(such as in the case of Cu vs Ag). In this case, the metal with a larger metal–metal bonding strength (in this example, Cu) tends to occupy the interstitial sites. The second case involves metals which have similar metal–metal bonding strengths but different electronegativities, as exemplified by Au vs Cu. In this case, the metal with a larger electronegativity (Au) will have a greater tendency to occupy the interstitial sites. The third case involves metals whose differences in both bonding strength and electronegativity are large and follow the same trend (e.g., Au vs Ag); then the metal with the larger metal–metal bonding strength and the larger electronegativity (i.e., Au) will occupy the interstitial sites. Finally, the fourth case, which is more difficult to ascertain, involves metals whose differences in bonding strength and in electronegativity follow opposite trends as in the case of Ni vs Au where metal–metal-bonding strength alone predicts that Ni will occupy the interstitial sites and electronegativity consideration alone favors Au as the interstitial atom. Obviously in this case the site preference depends on the relative energy stabilizations of both factors. In most cases, however, for transition metals, the former effect dominates (which predicts that Ni prefers the interstitial sites).

Finally, though difficult to quantify, we can use the bond energies calculated via eq 1 and shown in the BSCA plots (Figure 3) to predict the average metal–metal distances since the trends of these two variables are inversely related. For example, as shown in Figure 4 (which corresponds to Figure 3b), the five observed average metal–metal distances (in Å) in **1** follow the trend of Pt–Au (2.69) < Pt–Ag (2.81) < Au–Au (2.88) ~ Au–Ag (2.88) < Ag–Ag (2.90, 2.95) which correlates (in reverse order) with the corresponding trend of the bond energies (in kJ/mol): Pt–Au (77.83) > Pt–Ag (70.88) > Au–Au (61.37) > Au–Ag (54.43) > Ag–Ag (47.48). Similar correlations can also be obtained for the trimetallic Au–Ag–Ni clusters (note, however, Ni–Ag and Au–Au are similar in energies and hence have similar distances).

(B) Metal–Ligand Interactions: Bulk-to-Surface and Surface-to-Surface Segregations. It is well-known that the surface of bimetallic particles often has a different composition than its interior. Thermodynamic causes for this "surface enrichment" have been discussed in the literature.[11] There are also kinetic factors which favor certain arrangements of metal atoms in mixed-metal clusters. Metal–ligand interactions play an important role in dictating the surface composition of a multimetallic clusters. Here we may distinguish between two kinds of surface enrichment and/or segregation processes. The first type is analogous to the so-called "chemisorption-induced surface segregation"[25] whereby strong metal–ligand interactions cause a surface enrichment of metal atoms which would otherwise prefer interstitial (bulk) sites. For example, on the basis of the BSCA plot discussed in the previous section, Au–Pt alloy particles should have a Pt-rich core (kernel) and a Au-rich surface (mantle) due to the high cohesive energy of Pt vs Au. Exposure to a CO atmosphere, however, causes an enrichment of platinum atoms at the surface as a result of the strong and selective interactions between CO and the Pt atoms (and not to Au atoms). This results in a Au-rich core and a Pt-rich surface.[25a]

The second type of "surface segregation" is exemplified by the two title structures **1** and **4**. As discussed in section III(C), the more electronegative surface Au atoms prefer the more electron-donating phosphines as ligands whereas the less electronegative surface Ag atoms prefer coordination with the more electronegative halide ligands. In other words, selective metal–ligand bindings may cause segregation of Au and Ag atoms on the surface of a cluster.

In short, strong, selective metal–ligand bonding can cause either a "bulk-to-surface" inversion (first type) or a "surface-to-surface" segregation (second type).

(V) Conclusions

In conclusion, $[(Ph_3P)_{10}Au_{12}Ag_{12}PtCl_7]^+$ (**1**),[10] as the Cl^- salt, represents the first example of a trimetallic polyicosahedral supracluster. $[(Ph_3P)_{10}Au_{12}Ag_{12}NiCl_7]^+$ (**4**), as the SbF_6^- salt, represents the first Au–Ag–Ni compound ever reported as well as the first example of a vertex-sharing polyicosahedral cluster containing first, second, and third row transition metals. As such, they pave the way to other interesting trimetallic Au–Ag–M clusters (where M = group 10 metals such as Pt, Pd, Ni),[26] especially those of catalytic[11] and nanotechnological[12] importance.

(25) (a) Bouwman, R.; Sachtler, W. M. H. *J. Catal.* **1970**, *19*, 127. (b) Sinfelt, J. H. *Acc. Chem. Res.* **1987**, *20*, 134. (c) Williams, F. L.; Boudart, M. *J. Catal.* **1973**, *30*, 438.

(26) Work in progress.

Specifically, the new synthetic strategy (reductive addition of a third metal to a preformed bimetallic cluster) reported here, in combination with that already developed for the bimetallic (Au–Ag) system[5-9] ("cluster of clusters" approach), should allow a systematic design and preparation of various series of trimetallic Au–Ag–M (M = Pt, Pd, Ni)[26] clusters.

The bi- and trimetallic vertex-sharing biicosahedral sequences are depicted in Chart 1. The successful syntheses of **1** and **4** reported here suggest the existence of a parallel sequence of trimetallic (Au–Ag–M where M is a group 10 metal) vertex-sharing polyicosahedral supraclusters, from a single icosahedron of 13 metal atoms to an icosahedron of icosahedra of 127 metal atoms, in analogy to the bimetallic (Au–Ag) vertex-sharing polyicosahedral clusters.[5-9]

The observed site preference in **1** and **4** can be rationalized in terms of the disparities in metal–metal- vs metal–ligand-bonding strengths. As far as metal–metal bonding is concerned, the site preference rules established for these vertex-sharing polyicosahedral supraclusters can be understood with the aid of bond strength vs charge accumulation (BSCA) plots. Here the metal–metal-bonding strengths are estimated from the cohesive energy whereas the charge accumulation powers are based on Pauling's electronegativity. The site preferences, as indicated by the BSCA plots, can be extended to multimetallic phases. Here, in a general sense, each line connecting two metals in a BSCA plot represents variations of these two parameters (bond energy and electronegativity) for an admixture of the two metal constituents. The importance of metal–ligand bonding in dictating surface segregation and/or enrichment is also discussed. These qualitative pictures are supported by EHMO calculations. It is hoped that basic understanding of stereochemical and bonding principles governing site preference in multimetallic clusters will lead to better electronic and stereochemical controls of their structures and reactivities and, ultimately, to better design and manufacture or fabrication of structurally well-defined and functionally optimized multimetallic catalysts,[11] ultrafine particles, nanoarchitecture,[12] etc.

Acknowledgment is made to the National Science Foundation (CHE-9115278) for financial support of this research. We are also grateful to the staff of the Electron Microscope Facility, Research Resources Center at UIC, for technical assistance.

Supplementary Material Available: For $[(Ph_3P)_{10}Au_{12}Ag_{12}PtCl_7]Cl$ and $[(Ph_3P)_{10}Au_{12}Ag_{12}NiCl_7]SbF_6$, full listings of anisotropic thermal parameters (Table A), positional and thermal parameters for phenyl groups (Table B), and positional and thermal parameters for solvent atoms (Table C) for $[(Ph_3P)_{10}Au_{12}Ag_{12}PtCl_7]Cl$ and $[(Ph_3P)_{10}Au_{12}Ag_{12}NiCl_7]SbF_6$ (14 pages). Ordering information is given on any current masthead page.